

# Assessing acetone for the GISS ModelE2.1 Earth system model

Alexandra Rivera<sup>1</sup>, Kostas Tsigaridis<sup>2,3</sup>, Gregory Faluvegi<sup>2,3</sup>, Drew Shindell<sup>4</sup>

<sup>1</sup>Pratt School of Engineering, Duke University, Durham, NC, 27708, USA

<sup>2</sup>Center for Climate Systems Research, Columbia University, 2880 Broadway, New York, NY, 10025, USA

<sup>3</sup>NASA Goddard Institute for Space Studies, 2880 Broadway, New York, NY, 10025, USA

<sup>4</sup>Nicholas School of the Environment, Duke University, Durham, NC, 27708, USA

Correspondence to: Kostas Tsigaridis (kostas.tsigaridis@columbia.edu)

**Abstract.** Acetone is an abundant volatile organic compound (VOC) in the atmosphere with important influence on ozone and oxidation capacity. Direct sources include chemical production from other VOCs as well as anthropogenic emissions, terrestrial vegetation, biomass burning emissions, and ocean production. Sinks include chemical loss, deposition onto the land surface, and ocean uptake. Acetone also has a lifetime that is long enough to allow transport and reactions with other compounds remote from its sources. The NASA Goddard Institute for Space Studies (GISS) Earth System Model, ModelE2.1, simulates a variety of Earth system interactions. Previously, acetone had a very simplistic representation in the ModelE chemical scheme. This study assesses a more sophisticated acetone scheme in which acetone is a full 3-dimensional tracer with explicit sources, sinks, and atmospheric transport. We first evaluate the new global acetone budget in the context of past literature. Estimated source and sink fluxes fall within the range of previous models, although total atmospheric burden and lifetime fall on the lower end of published literature. Acetone's new representation in the ModelE2.1 also results in more realistic spatial and vertical distributions, which we compare against previous models and field observations. The seasonality of acetone-related processes was also studied in conjunction with field measurements, and these comparisons show promising agreement but have shortcomings at high-emission urban locations where the model's resolution is too coarse to capture the behavior. Finally, we conduct a variety of sensitivity studies that explore the influence of key parameters on the acetone budget and its global distribution. An impactful finding is that the production of acetone from precursor hydrocarbon oxidation has strong leverage on the overall chemical source, indicating the importance of accurate molar yields. Overall, our implementation is one that corroborates with previous studies and marks a significant improvement to the development of the acetone tracer in the GISS ModelE2.1.

## 1 Introduction

Acetone (C<sub>3</sub>H<sub>6</sub>O) is an abundant oxygenated volatile organic compound (VOC) that has important connections to ozone and the atmosphere's self-cleansing oxidation capacity (Read et al., 2012). Acetone's dynamic presence in Earth's atmosphere can be described through sources, sinks, and mechanisms of transport. Extensive literature has discussed the nature of these sources and sinks, and some are more well-constrained than others.

Primary sources of acetone in the atmosphere include anthropogenic, terrestrial vegetation, and biomass burning emissions. Past literature has found the fluxes of these sources to range between 1-2 Tg yr<sup>-1</sup>, 30-45 Tg yr<sup>-1</sup>, 2.5-4.5 Tg yr<sup>-1</sup>, respectively (Beale et al., 2013; Brewer et al., 2017; Elias et al., 2011; Fischer et al., 2012; Folberth et al., 2006; Jacob et al., 2002; Singh et al., 2000; Wang et al., 2020). Chemical production from other VOCs with 3 or more carbon atoms, each with their own molar yields, is another source of acetone in the atmosphere (Brewer et al., 2017; Fischbeck et al., 2017; Hu et al., 2013; Jacob et al., 2002; Singh et al., 2000; Weimer et al., 2017).

Deleted: anthropogenic

Deleted: ,

Deleted: oceanic, and

Deleted: . Acetone is also produced chemically from other volatile organic compounds

Deleted: surfaces

Deleted: , as well as chemical loss

Deleted: 's

Deleted: is

Deleted: latest

Deleted: ,

Deleted: .

Moved down [1]: We find the production of acetone from precursor hydrocarbon oxidation has strong leverage on the overall chemical source, indicating the importance of accurate molar yields for this source.

Deleted: . Anthropogenic emissions, vegetation emissions, biomass burning, and deposition representations agree well with previous studies. Chemistry and the ocean contribute to both sources and sinks of acetone, with their net values agreeing with the literature, although their individual source and sink terms appear to be overestimated for chemistry and underestimated for ocean fluxes.

Deleted: Spatial distributions reveal that ocean uptake of acetone is strongest in northern latitudes, while production is mainly in mid-southern latitudes.

Deleted:

Deleted: around the world

Deleted: . T

Deleted: ,

Deleted: ,

Deleted: since

Deleted: in high-emission areas

Moved (insertion) [1]

Deleted: We find

Deleted: , indicating the importance of

Deleted: s for this source

Deleted: analysis

Deleted: of the acetone budget

Deleted: aids the

Deleted: this

Deleted: , a crucial step to understanding the role of acetone in the atmosphere.

78

79 Sinks of acetone include wet and dry deposition, as well as chemical loss. Wet deposition occurs within and below clouds due to  
80 the solubility of acetone, and depends on its Henry's Law coefficient (Benkelberg et al., 1995). Dry deposition occurs on the land  
81 surface. Chemical loss of acetone forms radicals through photolysis. Past literature has estimated the acetone sinks to be 10-30%  
82 dry deposition, and 40-85% chemical loss (Arnold et al., 2005; Elias et al., 2011; Fischer et al., 2012; Khan et al., 2015; Singh et  
83 al., 1994). The estimated fluxes are 10-16 Tg yr<sup>-1</sup> and 45-60 Tg yr<sup>-1</sup> for total deposition and chemical loss, respectively (Arnold et  
84 al., 2005; Brewer et al., 2017; Dufour et al., 2016; Elias et al., 2011; Fischer et al., 2012; Jacob et al., 2002; Khan et al., 2015;  
85 Marandino et al., 2005; Singh et al., 2000; Wang et al., 2020).

86

87 The ocean surface is a bidirectional flux that provides both a source and a sink for acetone. Ocean surface conditions such as wind  
88 speed, sea surface temperature, and seawater concentration of acetone can influence the direction and magnitude of ocean-acetone  
89 exchange (Wang et al., 2020). Previous literature estimates an oceanic source flux of 25–50 Tg yr<sup>-1</sup> and oceanic uptake flux of  
90 35–60 Tg yr<sup>-1</sup>. However, there is little consensus in the literature on whether the ocean serves as a net source or sink of acetone,  
91 with some studies indicating a net oceanic source (Beale et al., 2013; Jacob et al., 2002; Wang et al., 2020), and other studies  
92 indicating a net oceanic sink (Brewer et al., 2017; Elias et al., 2011; Fischer et al., 2012; Wang et al., 2020).

93

94 In addition to a global annual mean atmospheric budget, previous studies have reported the seasonality of acetone-related processes.  
95 Past studies have compared monthly estimates of acetone mixing ratios to field measurements of European sites from Solberg et  
96 al. (1996) (Arnold et al., 2005; Elias et al., 2011; Jacob et al., 2002). Comparisons with these European sites have emphasized the  
97 seasonal variability of acetone emissions, as nearly all sites portray a summer maximum and winter minimum of acetone  
98 abundance. Vegetation emissions from June to September, along with chemical sources, have an especially strong contribution to  
99 this seasonality. The winter minimum of acetone is aided by an ocean sink at coastal sites (Jacob et al., 2002).

00

01 Other studies have described spatial distributions and seasonal dependence of ocean fluxes of acetone (Fischer et al., 2012; Wang  
02 et al., 2020). A model by Fischer et al. (2012) proposed a net ocean sink of 2 Tg yr<sup>-1</sup> and characterized ocean uptake of acetone as  
03 strongest in northern latitudes year-round and in the high southern latitudes during the winter. An oceanic acetone source was  
04 dominant in the tropical regions, with an exception off the western coasts of Central America and Central Africa (Fischer et al.,  
05 2012). A model by Wang et al. (2020) that varied surface seawater acetone concentration through a machine learning approach  
06 also proposed a net ocean sink year-round. This net sink was strongest in December-February, and weakest in March-May.

07

08 The vertical distribution of acetone has been modeled between the seasons of May-October and November-April in the surface  
09 and troposphere (Fischer et al., 2012). Acetone concentrations are generally higher in the lower altitudes due to proximity to surface  
10 emissions. Surface-level acetone has been measured over a variety of terrestrial and oceanic sites around the world (de Gouw et  
11 al., 2004; Dolgorouky et al., 2012; Galbally et al., 2007; Guérette et al., 2019; Hu et al., 2013; Huang et al., 2020; Langford et al.,  
12 2010; Lewis et al., 2005; Li et al., 2019; Read et al., 2012; Schade and Goldstein, 2006; Singh et al., 2003; Solberg et al., 1996;  
13 Warneke and de Gouw, 2001; Yoshino et al., 2012; Yuan et al., 2013), and in some cases, these measurements were taken over a  
14 variety of months to provide a sense of seasonality (Dolgorouky et al., 2012; Hu et al., 2013; Read et al., 2012; Schade and  
15 Goldstein, 2006; Solberg et al., 1996). Additionally, vertical distributions of acetone have been measured through NASA's  
16 Atmospheric Tomography Mission (ATom) campaigns (Thompson et al., 2022). The ATom-1, ATom-2, ATom-3, and ATom-4  
17 campaigns took place during July-August 2016, January-February 2017, September-October 2017, and April-May 2018,

Deleted: onto the land surface

Deleted: ,

Deleted: w

Deleted: 1

22 respectively. Each campaign provided mixing ratios for a variety of VOCs in profiles from the marine boundary layer up to the  
23 upper troposphere/lower stratosphere (Apel et al., 2021).

24  
25 The NASA Goddard Institute for Space Studies (GISS) ModelE2.1 Earth System Model (Kelley et al., 2020) has the capability of  
26 simulating a variety of Earth system interactions, is used both to interpret and predict past and future climate, and routinely  
27 participates in the Climate Model Intercomparison Projects (CMIP) and Intergovernmental Panel for Climate Change (IPCC)  
28 reports. Here we used and enhanced this model by adding acetone as an independent chemical tracer (Kelley et al., 2020).  
29 Previously, acetone had a very simplistic representation in the model's chemical scheme (Shindell et al., 2003), in which acetone's  
30 spatial variation was parameterized based on the difference of the model's zonal mean distribution of isoprene and that tracer's  
31 three-dimensional distribution. Acetone's lifetime is long enough to be transported remote from sources, but not long enough to  
32 become uniformly mixed, and therefore its simulated distribution should benefit from a more realistic implementation. We  
33 developed a greatly improved acetone tracer scheme by making prognostic calculations of the 3-dimensional distribution of acetone  
34 as a function of time. We evaluated its atmospheric burden and lifetime as well as source/sink fluxes (anthropogenic emissions,  
35 vegetation emissions, biomass burning, deposition, ocean, and chemistry) against other models and its concentration against field  
36 measurements. This work aims to provide a holistic assessment of the abundance of acetone in the atmosphere.

## 37 **2 Methodology**

38 Here we implement acetone in the GISS ModelE2.1 based on the literature rather than developing a new parameterization. Our  
39 'Baseline' simulation is a climatological mean with year 2000 conditions, chosen to be relatively modern without precluding  
40 comparison with models in older literature. The 1996-2004 mean of prescribed emissions from Hoesly et al. (2018) were used,  
41 along with the 1996-2005 mean sea surface temperature and sea ice cover as described in Kelley et al. (2020). Acetone simulations  
42 use full chemistry and not archived OH fields. An additional simulation, 'Nudged\_ATOM', was conducted to compare more directly  
43 with ATom field measurements. This simulation employed nudged winds from MERRA2 (Gelaro et al., 2017), ocean surface  
44 conditions [from PCMDI-AMIP 1.1.4 for 2016-2017](#) (Taylor et al., 2000) [and from Hadley Center HadISST1.1 for 2018](#) (Met  
45 Office, Hadley Centre, 2006), and trace gas and aerosol emissions changing with time during 2016-2018.

### 46 **2.1 Sources**

#### 47 **2.1.1 Anthropogenic emissions**

48 Anthropogenic emissions were prescribed using the 1996-2004 averages of the Community Emissions Data System (CEDS)  
49 emissions from Hoesly et al. (2018) as prepared for the GISS contributions to the Coupled Model Intercomparison Project, Phase  
50 6 (CMIP6) (Kelley et al., 2020). These include sources from agriculture, the energy sector, the industrial sector,  
51 residential/commercial/other, international shipping, solvents production and application, the transportation sector, and waste. In  
52 line with past studies, we base acetone emissions on that of ketones. VOC23-ketones emissions from Hoesly et al. (2018) were  
53 scaled down by a ratio of acetone molecular weight to an average ketone molecular weight ( $58.08 \text{ g mol}^{-1}/75.3 \text{ g mol}^{-1}$ ).  
54 Maintaining the resulting spatial and temporal pattern of emissions, the magnitudes were then tuned to be close to that of Fischer  
55 et al. (2012), resulting in a total of about  $1 \text{ Tg yr}^{-1}$ . This resulted in roughly 36.5% of CEDS VOC23-ketones used as acetone  
56 emissions. Lacking an accurate way to obtain acetone aircraft emissions from the bulk VOCs available in the emission inventory,  
57 we have neglected that sector in the simulations.

58 **2.1.2 Terrestrial vegetation emissions**

59 Emissions from land vegetation were derived from the Model Emissions of Gases and Aerosols from Nature (MEGAN), version  
60 2.1 (Guenther et al., 2012), a new contribution to the ModelE. Emission response algorithms in the MEGAN2.1 model are derived  
61 from input leaf area indices, solar radiation, temperature, moisture, CO<sub>2</sub> concentrations, and plant functional types and composition  
62 of species (Guenther et al., 2012). The acetone vegetation emissions in the Baseline simulation in GISS ModelE2.1 were calculated  
63 to equal 36.1 Tg yr<sup>-1</sup>.

Deleted: are

64 **2.1.3 Biomass burning emissions**

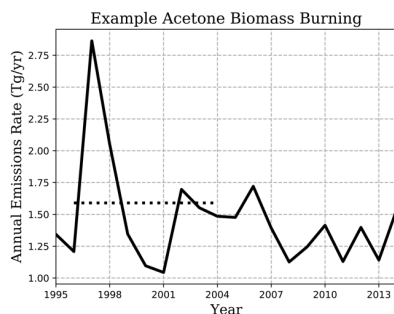
65 Acetone emissions were prescribed from a 1996-2004 average of the NMVOC-C<sub>3</sub>H<sub>6</sub>O species from version 2.1 of the biomass  
66 burning dataset of van Marle et al. (2017), used by CMIP6. The acetone mass flux from biomass burning in the Baseline simulation  
67 was 1.59 Tg yr<sup>-1</sup>.

68  
69 Figure 1 shows the biomass burning emission rate chosen for this study, and how it lies within the range of substantial interannual  
70 variation. During the 20-year period shown, emissions averaged 1.46 Tg yr<sup>-1</sup>, with a standard deviation of 0.402, and a spike in the  
71 earlier years of emissions over 2.75 Tg yr<sup>-1</sup> is also observed (Figure 1). On top of any differences across emission inventories, the  
72 years considered when reporting emissions may be the reason for disagreements between models (e.g. 2.40 – 2.80 Tg yr<sup>-1</sup> from the  
73 2006 GFED-v2 emission inventory in Elias et al. (2011) and Fischer et al. (2012), compared to 3.22 Tg yr<sup>-1</sup> from 1997-2001 in  
74 Folberth et al. (2006)).

Deleted: variability

Deleted: 3

Deleted: variability



75  
76 **Figure 1.** Illustration of interannual variation of NMVOC-C<sub>3</sub>H<sub>6</sub>O biomass burning emissions of van Marle et al. (2017) (solid  
77 line), used as acetone emissions in our simulation. Climatological-emissions simulations use the 1996-2004 mean (dotted line),  
78 though emissions vary by month.

Deleted: variability

79 **2.2 Sinks**

80 **2.2.1 Deposition**

81 Both dry and wet deposition of acetone were included in the model, although dry deposition was, on average, 91% of total  
82 deposition. The wet deposition scheme is given by Koch et al. (1999). Acetone and other species are transported within and below  
83 clouds, and soluble gases are deposited depending on the conditions of the grid box they are in and a Henry's Law Coefficient  
84 (Shindell et al., 2001). The Henry's Law Coefficient for acetone used in the GISS ModelE2.1 is 27 mol L<sup>-1</sup> atm<sup>-1</sup>, with a Henry  
85 temperature dependence of acetone of 5300 J mol<sup>-1</sup> (Benkelberg et al., 1995; Zhou and Mopper, 1990). The dry deposition scheme

91 uses resistance-in-series calculations, global seasonal vegetation data (Chin et al., 1996; Shindell et al., 2001; Wesely and Hicks,  
92 1977), and a reactivity factor of  $f_0=0.1$ . This resulted in an acetone deposition rate in the Baseline simulation of  $22.2 \text{ Tg yr}^{-1}$ .

### 93 2.3 Chemistry

94 The GISS ModelE2.1 Baseline simulation estimates a net chemistry flux of  $-20.6 \text{ Tg yr}^{-1}$ . The components can be broken up into  
95 sources and sinks as follows.

Deleted: change

#### 96 2.3.1 Chemical sources

97 The Baseline simulation estimates chemical production to be  $33.3 \text{ Tg yr}^{-1}$ . The acetone chemical scheme includes two production  
98 reactions:



101 In the first reaction, acetone is produced by paraffin, a proxy tracer for paraffinic (saturated) carbon, and OH (Eq. 1). The molar  
102 yield of acetone from paraffin was found to be a strong leverage to the overall chemical source (see Section 3.5). A rate coefficient  
103 of  $8.1 \times 10^{-13} \text{ cm}^3 \text{ molecule}^{-1} \text{ s}^{-1}$  was used (Shindell et al., 2003). Previous literature has suggested an acetone yield on a molecular  
104 scale of 0.72 (Fischbeck et al., 2017; Jacob et al., 2002; Weimer et al., 2017). Initial tests using a yield of 0.72 resulted in an  
105 overestimated chemistry source, leading us to re-evaluate this yield for the specific mixture of VOCs represented in the GISS  
106 ModelE2.1.

Deleted: E-13

107 Our model's anthropogenic emissions of paraffin is based on an aggregation of selected VOC groups. Based on year 2019 emissions  
108 of the O'Rourke et al. (2021) dataset, we emit paraffin that is about 11% propane by mole, 22% butane and 21% pentane.  
109 Multiplying these by each VOC's acetone molar yield (0.73, 0.95, 0.63, respectively), we estimate that 42% of paraffin from  
110 anthropogenic sources becomes acetone in our model. Paraffin biomass burning emissions, estimated from year 2020 of SSP3\_70  
111 emissions (Riahi et al., 2017; Fujimori et al., 2017) contain mole fractions for propane of 9% and higher alkanes of 23%, and when  
112 multiplied by acetone molar yields of 0.73 and 0.79, respectively, suggest that about 25% of paraffin from biomass burning sources  
113 becomes acetone in our model. The molar yields used in these calculations were derived with suggestions from the literature  
114 (Fischbeck et al., 2017; Jacob et al., 2002; Weimer et al., 2017). Refer to the "Chemical sources" section of the manuscript  
115 supplement for a more detailed breakdown. Overall, an average of the 42% anthropogenic paraffin and 25% biomass burning  
116 paraffin was used to conclude that approximately 35% of paraffin from emissions becomes acetone, leading to our refinement of  
117 the molar yield in Eq. (1) to 0.35.

118 Additionally, reactions between terpenes and  $\{\text{OH}, \text{O}_3\}$  were implemented with an acetone yield of 0.12 (Hu et al., 2013; Jacob et  
119 al., 2002) (Eq. 2). The rates for these reactions are  $2.51 \times 10^{-11} e^{(444/T)} \text{ cm}^3 \text{ molecule}^{-1} \text{ s}^{-1}$  for the OH reaction and  $1.40 \times 10^{-14} e^{(-732/T)}$   
120  $\text{cm}^3 \text{ molecule}^{-1} \text{ s}^{-1}$  for the  $\text{O}_3$  reaction, and these coefficients are enhanced from the standard  $\alpha$ -pinene one to consider the reactivity  
121 variability across mono- and higher terpenes (Tsigaridis and Kanakidou, 2003).

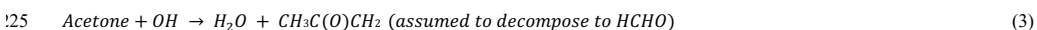
Deleted:  $2.51 \times 10^{-11} \exp(444/T)$

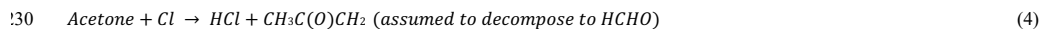
Formatted: Superscript

Deleted:  $1.40 \times 10^{-14} \exp(-732/T)$

#### 122 2.3.2 Chemical sinks

123 The chemical sink of acetone in the Baseline simulation is estimated to be  $53.8 \text{ Tg yr}^{-1}$ . The sinks of acetone include oxidation by  
124 OH and Cl radicals, and photolysis:





133 The first and second acetone destruction reactions above have rates of  $1.33 \times 10^{-13} + 3.82 \times 10^{-11} e^{(-2000/T)}$  cm<sup>3</sup> molecule<sup>-1</sup> s<sup>-1</sup> and  
134  $7.70 \times 10^{-11} e^{(-1000/T)}$  cm<sup>3</sup> molecule<sup>-1</sup> s<sup>-1</sup>, respectively (Sander et al., 2011) (Eq. 3, 4). Previously, acetone photolysis (which only  
135 affected production of radicals and not acetone itself) did not utilize the model's photolysis scheme but was parameterized solely  
136 as a function of orbital geometry and atmospheric pressure. In the model updates, photolysis now consists of two separate reactions,  
137 where acetone forms either CH<sub>3</sub>CO + CH<sub>3</sub> radicals or two CH<sub>3</sub> radicals and CO (Eq. 5, 6). The spectroscopic data used for acetone  
138 photolysis is from JPL 2010 (Sander et al., 2011) and mapped onto Fast-J version 6.8d's wavelength intervals (Neu et al., 2007).  
139 The photolysis cross section for Eq. 5 is pressure-dependent while that of Eq. 6 is temperature-dependent, leading to variation in  
140 yields with altitude and location. For example, in a standard atmosphere the ratio of the yield of CO to CH<sub>3</sub>CO decreases from  
141 0.28 at the surface to 0.18 at 4 km altitude.

## 142 2.4 Ocean

143 Bidirectional fluxes of acetone are calculated over ocean based on the "two-phase" model of molecular gas exchange at the air-sea  
144 interface of Liss & Slater (1974), as it is described in Johnson (2010). The fluxes are a function of simulated surface temperature  
145 and near-surface wind speed but independent of salinity. Henry's Law constants and temperature dependence of solubility for  
146 acetone are from Sander (1999). The source from ocean water and sink from the atmosphere are calculated assuming a constant  
147 concentration of acetone in water (of 15 nM), the lower boundary layer atmospheric concentration, and the total transfer velocity  
148 (a combination of water-side and air-side transfer velocities). The constant concentration of 15 nM follows the implementation by  
149 Fischer et al. (2012) in the GEOS-CHEM model, who looked at observations and did not find a strong reasoning to make the  
150 concentration vary seasonally or spatially. The GISS ModelE2.1 Baseline simulation calculates the ocean to be a net source of  
151 acetone, producing 3.94 Tg yr<sup>-1</sup>.

## 152 2.5 Sensitivity studies

153 Sensitivity studies were conducted to determine the influence of key parameters on the acetone budget and its global distribution  
154 (summarized in Table 1). Specifically, we were interested in seeing the sensitivity of simulated acetone to artificial perturbations  
155 in given parameters. Sensitivity studies for chemistry modify the production of acetone. The Chem Cl0 and Chem Terp0  
156 simulations provide no formation of acetone from chlorine or terpenes, respectively. The importance of paraffin is explored by  
157 halving its yield of acetone to 17.5% in the Chem\_Par0.5 simulation, and by doubling its yield of acetone to 70% in the  
158 Chem\_Par2.0 simulation. As vegetation was the most prominent source of acetone, the Veg 0.7 simulation observes its reduction  
159 by decreasing the MEGAN production of acetone by 30%. The Ocn\_2.0 simulation aims to explore the impact of ocean acetone  
160 concentration by doubling it from 15 nM to 30 nM globally. The Dep\_f0 simulation tests dropping the reactivity factor for dry  
161 deposition from 0.1 to 0. Finally, given the high interannual variability of biomass burning emissions, the BB\_2.0 simulation  
162 explores the impact of doubling those emissions.

164 **Table 1.** Sensitivity studies conducted to observe the leverage that a specific parameter afforded the model. Simulation names, as  
165 well as the parameter they target and a description, are included.

Deleted:  $1.33E-13 + 3.82E-11 * \exp(-2000/T)$

Deleted:  $7.70E-11 * \exp(-1000/T)$

Deleted: Reaction 5 is pressure-dependent, while reaction 6 is temperature-dependent. The spectroscopic data used for acetone photolysis is from

Deleted: quantum yields

Deleted: are pressure and temperature dependent and thus vary with altitude and location

Deleted: atmospheric

Deleted: in seeing how much leverage a given parameter afforded the model by way of an artificial perturbation

Deleted: sources

Deleted: ,

Deleted: tested

Deleted: zero



Chemical Lifetime (days) <sup>c</sup>	19.9	25.8	26.6	43.6	39.3	32.9	19.0	20.9 – 35.6
Lifetime (days) <sup>d</sup>	12.3	11.0	12.7	17.2	14.0	21.0	14.5	12.8 – 35.0

<sup>a</sup> CAM-Chem Model (Wang et al., 2020)

<sup>b</sup> GEOS-Chem Model (Wang et al., 2020)

<sup>c</sup> Chemical Lifetime = Burden/Chemical Sink

<sup>d</sup> Total Atmospheric Lifetime = Burden/Total Sink

<sup>e</sup> Singh et al. [2000, 2004], Arnold et al. [2005], Folberth et al. [2006], Marandino et al. [2006], Guenther et al. [2012], Beale et al. [2013], Khan et al. [2015], Dufour et al. [2016].

i20

i21 Atmospheric burden describes the total amount of acetone that is in the atmosphere. The GISS ModelE2.1 Baseline simulation  
i22 estimates the burden to be 2.93 Tg. Additionally, chemical lifetime and atmospheric lifetime can be derived from burden. The  
i23 chemical lifetime of acetone is calculated as the burden divided by the chemical sink, whereas total lifetime is the burden divided  
i24 by all sinks. The chemical and total atmospheric lifetimes for the Baseline simulation are calculated to be 19.9 and 12.3 days,  
i25 respectively. These values are also placed in the context of previous literature in Table 2.

i26

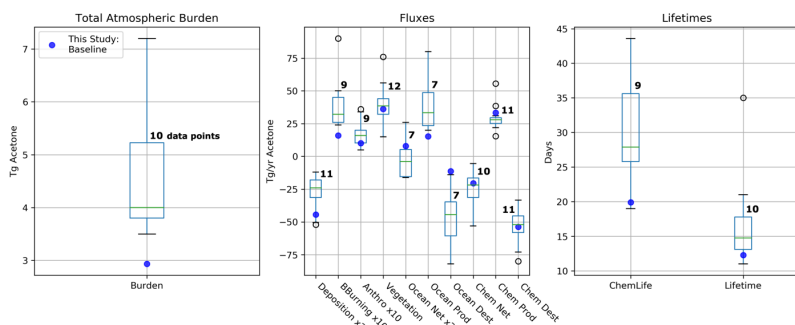
i27 The GISS ModelE2.1 Baseline acetone budget is further compared to previous model studies in Figure 2. The calculated fluxes in  
i28 ~~the~~ Baseline simulation that are less than one standard deviation away from the literature mean include anthropogenic and  
i29 vegetation emissions, net ocean, net chemistry, chemical production, and chemical destruction (Figure S1). Biomass burning in  
i30 GISS ModelE2.1 appears as an outlier when compared against 9 previous model studies but can be attributed to the high interannual  
i31 ~~variation~~ with emissions (as discussed in Section 2.1.3). The value of acetone deposition is on the high (more negative) end in  
i32 GISS ModelE2.1 relative to 11 previous studies. This might be partially attributed to differences in deposition parametrization  
i33 across models, as explored by our sensitivity study on dry deposition presented in Section 3.5.2. The values for oceanic acetone  
i34 sources and losses are smaller (in absolute values) than the mean from 7 previous model studies. Nevertheless, the net ocean flux  
i35 matches the literature well. Lastly, the total atmospheric burden and lifetime calculated by GISS ModelE2.1 are lower than the  
i36 previous papers, an expected consequence of the higher removal by deposition. The chemical lifetime is also calculated to be at  
i37 the low end of published literature.

Deleted: our

Deleted: variability

Deleted: section

Deleted: As the burden is a function of many different atmospheric parameters, however, it was not the goal to corroborate our estimates with the literature as much as it was for each of the fluxes. ...



i38

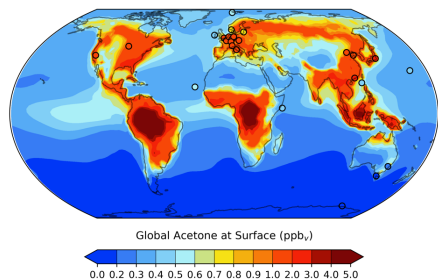
i39 **Figure 2.** Total atmospheric burden, fluxes, and lifetimes of acetone from the literature values in Table 2 (shown in boxes and  
i40 whiskers with outliers as open circles), and values from GISS ModelE2.1 (shown as solid blue circles). The number of models  
i41 used to create each box and whisker plot are labeled. Note that ~~the~~ deposition and ocean net fluxes were multiplied by 2 and ~~that~~  
i42 ~~the~~ biomass burning and anthropogenic emissions were multiplied by 10 for a better visualization of the distribution.

Deleted: 1



151 **3.2 Spatial distribution of acetone**

152 The global distribution of acetone at the surface is given in Figure 3. It is evident that acetone mixing ratios are largest over the  
153 continents, where anthropogenic, vegetation, and other terrestrial sources are located. Over the ocean, acetone mixing ratios are  
154 highest downwind of Central America and Central Africa. A comparison of the GISS ModelE2.1 results against twenty-six prior  
155 field measurements shows an overall great agreement, with a root mean squared error of 0.3494 and an R<sup>2</sup> value of 0.8306. To put  
156 these results into the context of model evaluation, a similar comparison to field measurements was done for the model's previous  
157 acetone scheme. The prior parameterization was designed as a rough representation of acetone oxidized from isoprene in the upper  
158 troposphere, without regard for realism near the surface, and this is evident from the comparison with surface observations: a root  
159 mean squared error and R<sup>2</sup> value of 1.3620 and 0.0413, respectively. The improvement of the new acetone tracer model in the  
160 GISS ModelE2.1 is evident from these statistics.



161 **Figure 3.** GISS ModelE2.1 spatial distribution of annual mean acetone at surface for the Baseline simulation. Filled circles  
162 represent data from twenty-six field measurements (de Gouw et al., 2004; Dolgorouky et al., 2012; Galbally et al., 2007; Guérette  
163 et al., 2019; Hu et al., 2013; Huang et al., 2020; Langford et al., 2010; Lewis et al., 2005; Li et al., 2019; Read et al., 2012; Schade  
164 & Goldstein, 2006; Singh et al., 2003; Solberg et al., 1996; Warneke & de Gouw, 2001; Yoshino et al., 2012; Yuan et al., 2013).  
165 The root mean squared error and the R<sup>2</sup> value between the Baseline acetone estimations and the field measurements are 0.3494  
166 and 0.8306, respectively. A nonlinear colorbar is used to better differentiate the details in the map.

168 A breakdown of the acetone bidirectional fluxes indicates that its chemical production is concentrated over the continents, while  
169 chemical destruction is primarily over the oceans (Figure 4). Hotspots of production over the continents include the Southeastern  
170 United States and Central South America, East and Northern Asia, and Central Africa. Chemical sinks over the oceans are stronger  
171 in the tropics than in the high southern or northern latitudes. Annually, there is a net flux of about -20.46 Tg yr<sup>-1</sup>. Observing the  
172 chemical flux across all four seasons, the net loss appears unaffected while the net source changes more significantly, following  
173 the seasonality of precursor compounds like isoprene and terpenes (Figure 4). Chemical production is strongest in the months of  
174 June/July/August, primarily in North America and Northern Asia. Production is weakest in the months of  
175 December/January/February, losing almost all production in North America and Northern Asia entirely. Still, a net negative flux  
176 is present for all four seasons (Figure 4).

Deleted: central

Deleted: central

Deleted: (Figure 4)

Deleted: rn and Eastern

Deleted: central

Deleted: negative

Deleted: (Figure 4)

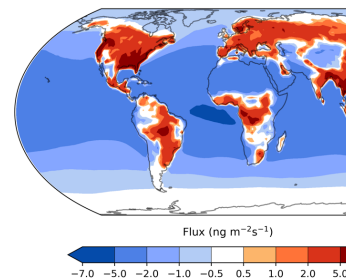
Deleted: over

Deleted: 5

Deleted: the US

Deleted: the US

Deleted: 5



Deleted:  
Figure 4. Annual average of acetone net chemistry fluxes (column-integrated) in the Baseline simulation, with red indicating a net source and blue indicating a net sink. A nonlinear colorbar is used to better differentiate the details in the map. The weighted global mean of the net chemistry flux is shown in a box on the lower right.

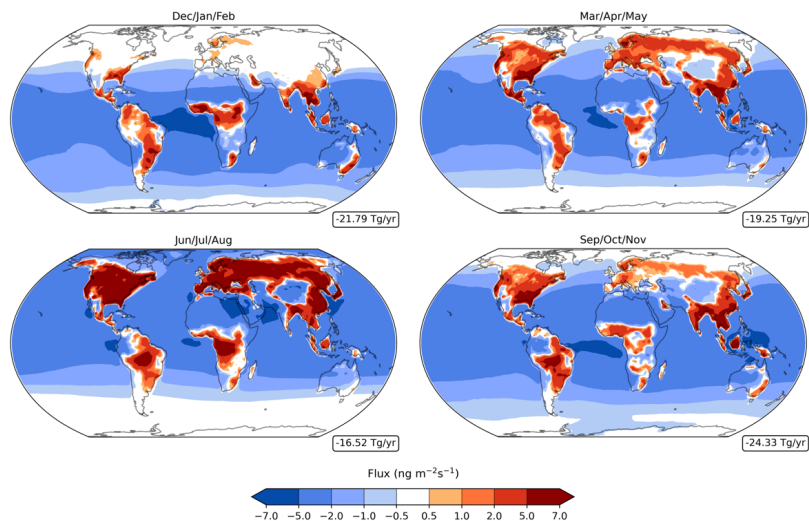
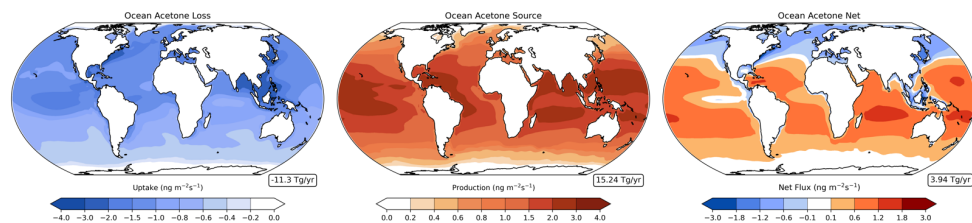


Figure 4. Net acetone chemistry fluxes (column-integrated) in the Baseline simulation for December-February (top left), March-May (top right), June-August (bottom left), and September-November (bottom right), with red indicating a net source and blue indicating a net sink. Nonlinear colorbars are used to better differentiate the details in the map. The weighted global means of the net chemistry fluxes are shown in boxes on the lower right of each subplot.

The ocean acetone sources and sinks are unevenly distributed across latitudes (Figure 5). Oceanic uptake of acetone is mostly concentrated in the northern rather than the southern oceans, while the ocean acetone source is strongest in the tropics and decreases at higher latitudes of both hemispheres. Combining these two unidirectional fluxes results in the ocean serving as a sink in the northern high latitudes, a source in the tropical latitudes, and near neutral at the high southern latitudes (Figure 5). This finding corroborates very well with findings from Fischer et al. (2012) and Wang et al. (2020). Additionally, oceanic bidirectional fluxes of acetone present trends over the four seasons (Figure S2). Overall, every season has a positive global mean net flux. However, production becomes strongest in the months of December through May, and weakest in the months of June through November. Off the coast of western South America, the ocean appears to be a net sink of acetone, even though this latitude band is generally a source of acetone (Figure 5, Figure S2). This is especially evident in the months of June/July/August and September/October/November. As the model simulates this location to have high levels of acetone at the surface (Figure 3), we believe the acetone in the air is driving the ocean to be a sink there.



Deleted: 5  
Deleted: Acetone net

Deleted: (Figure 6)  
Deleted: 7  
Deleted: Oceanic  
Deleted: acetone

Figure 5. Annual mean oceanic acetone uptake (left), oceanic acetone production (middle), and net bidirectional flux (right) in the Baseline simulation, with red indicating a net source and blue indicating a net sink. Nonlinear colorbars are used to better differentiate the details in the map. The corresponding weighted global means of the ocean fluxes are shown in boxes on the lower right of each subplot.

### 3.3 Vertical distribution of acetone

The vertical distribution of acetone varies by latitude, with near-surface air mixing ratios being higher in the tropics and in the northern midlatitudes (Figure 6). Acetone levels in the atmosphere decrease with height, a direct result of sinks dominating the sources. Prior to the implementation of an acetone tracer in the GISS ModelE2.1, when acetone was derived from the zonal mean of isoprene, the vertical distribution looked very different. Acetone was only concentrated around the tropics and did not extend nearly as high into the troposphere. The complexity of Figure 6 supports the new acetone tracer scheme as a significant improvement to the GISS ModelE.

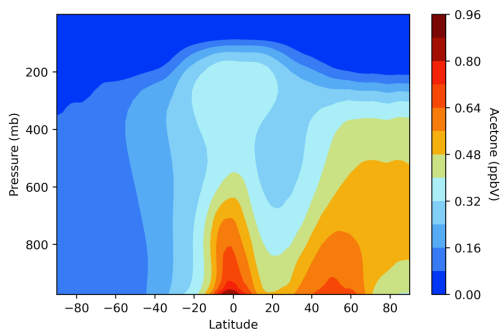
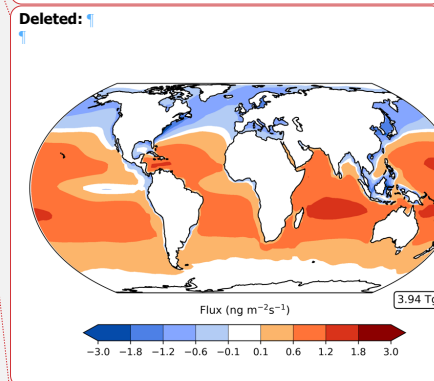


Figure 6. GISS ModelE2.1 vertical distribution of acetone air mixing ratios across latitudes in the Baseline simulation.

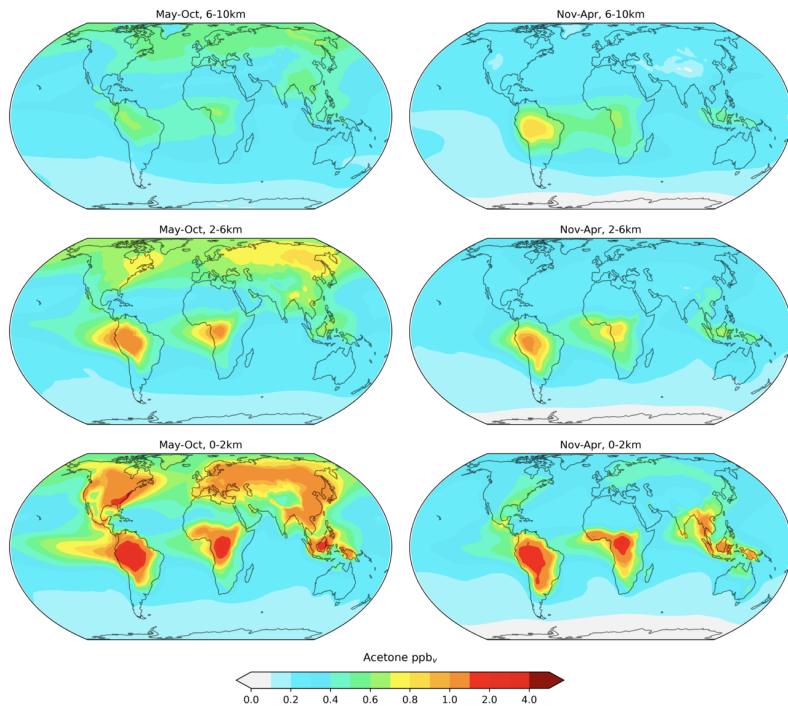
Another modeled vertical distribution of acetone, including a differentiation between two long seasons, is explored in Figure 7. In general, it was found that acetone mixing ratios are higher in the months of May-October than in November-April, and that this relationship is stronger in the lower atmosphere (0-2 km) than the upper atmosphere (6-10 km). This finding corroborated well with a similar analysis done by Fischer et al. (2012).

- Deleted: 6
- Deleted: average
- Deleted: of
- Deleted: the acetone
- Deleted: loss
- Deleted: and ocean
- Deleted: source
- Deleted: right
- Deleted: .



Deleted: Figure 7. Annual average of acetone ocean bidirectional fluxes in the Baseline simulation, with red indicating a net source and blue indicating a net sink. A nonlinear colorbar is used to better differentiate the details in the map. The weighted global mean of the net chemistry flux is shown in a box on the lower right.

- Deleted: (Figure 8)
- Deleted: atmosphere
- Deleted: 8
- Deleted: 8
- Deleted: 1
- Deleted: 9



162

163 **Figure 7.** Baseline simulation acetone mixing ratios in the atmosphere at approximately 0-2 km (bottom), 2-6 km (middle), and 6-  
 164 10 km (top) for the months of May-October (left) and November-April (right). The average mixing ratios over these broad altitude  
 165 layers are weighted by the air mass in the model layers they contain. The choice of the slices and colors match those in Figure 1  
 166 by (Fischer et al., 2012).

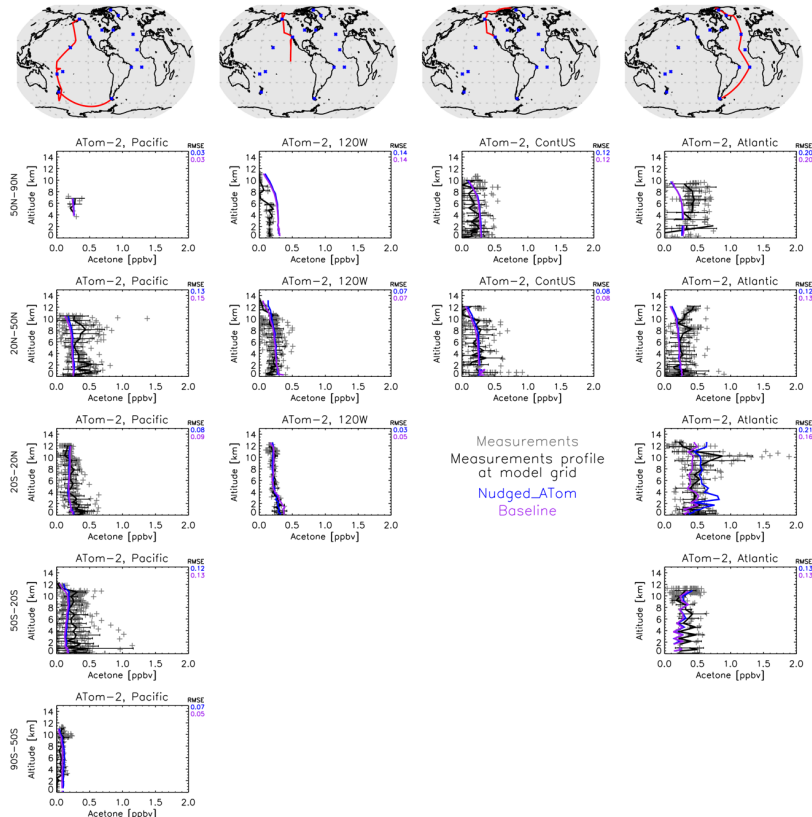
167

168 Additionally, the GISS ModelE2.1 was compared to four ATom campaigns (Thompson et al., 2022) of acetone field measurements  
 169 in the atmosphere (Apel et al., 2021). For this comparison, we averaged the flight data to the model grid, and then compared the  
 170 resulting mean against the monthly mean fields of the model output. Contrary to other chemical species measured during ATom  
 171 that vary significantly in space and time, acetone has a rather long lifetime, and the data are collected for the most part very far  
 172 from its sources. Combining that with the fact that prescribed emissions in the model vary by month, not by day or even hour in  
 173 GISS ModelE2.1, makes such a comparison appropriate. Meteorology though can affect long-range transport significantly, so for  
 174 that reason we performed a nudged simulation (called Nudged\_ATOM) towards the MERRA-2 reanalysis (Gelaro et al., 2017), to  
 175 capture such an effect more accurately. We also used emissions and greenhouse gas concentrations from the years of the ATom  
 176 campaigns and varying with year, rather than the climatological means used in the Baseline simulation. Both the Nudged\_ATOM  
 177 and Baseline simulations are plotted in the ATom comparisons presented here (Figure 8).

Deleted: 9

Deleted: in the vertical were averaged with an arithmetic mean

Deleted: 10



181  
 182 **Figure 8.** Comparison between the GISS ModelE2.1 simulations (Baseline in purple and Nudged\_ATOM in blue) and the ATom-  
 183 2 field measurements (January-February 2017). Individual data points are shown with dark grey symbols, and their average values  
 184 are shown in black, with error bars representing the one-sigma range of the averages. The root mean square error (RMSE) of each  
 185 simulation is noted at the top right of each subplot.

186  
 187 There are very few notable differences between the nudged and climatological simulations. An example is the tropical Atlantic  
 188 Ocean, where during ATom-2 (Figure 8), the nudged simulation calculates higher acetone concentrations, but without gain of skill.  
 189 Both model simulations miss the upper tropospheric peak that is found in the measurements, likely indicating a missing long-range  
 190 transported plume. There is a similar result for ATom-3 (Figure S4) for the southern Atlantic Ocean mid-latitudes, where the  
 191 nudged simulation is higher. Contrary to the ATom-2 case, both simulations for the ATom-3 case calculate an upper tropospheric  
 192 maximum, which is not found in the measurements. The tropical and southern mid-latitude Atlantic Ocean regions are both  
 193 downwind of African biomass burning zones during ATom-2 and ATom-3, respectively, hinting to a primary and/or secondary  
 194 incorrect source of acetone related with biomass burning and subsequent long-range transport. Other than those few cases, for the  
 195 most part the two simulations are indistinguishable, indicating that our conclusions comparing climatological simulations to ATom

- Deleted: 10
- Deleted: dot
- Deleted: s
- Deleted: shown
- Deleted: 10
- Deleted: Something
- Deleted: is calculated during
- Deleted: ,
- Deleted: regions

should be robust. (Figure 8, Figures S3-S5). This is important to remember in Section 3.5.3, where we perform sensitivity analyses using climatological simulations and comparing against all four ATom campaigns.

Deleted: s  
Deleted: 10  
Deleted: and

### 3.4 Seasonality of acetone

Most European sites presented in Figure 3 have monthly-resolved measurements that can be used to analyze the seasonal behavior of acetone in the model (Figure 9, Figure S6) (Solberg et al., 1996). These sites differ with respect to their geographic locations and their proximity to anthropogenic sources. Zeppelin, Birkenes, Rucava, and Mace Head are all coastal sites, while Waldhof, Kosetice, Donon, Ispra, and Montelibretti are inland sites. Regarding anthropogenic sources, Zeppelin is the most remote location and Birkenes and Rucava each have small sources. Mace Head is a site affected by the marine boundary layer, and Waldhof, Kosetice and Donon are sites with small local anthropogenic sources that are generally located in higher emission regions. Montelibretti and particularly Ispra are subject to the highest anthropogenic sources. The measurements taken at Ispra show an opposite seasonality than what is expected, and previous studies have considered this anomalous (Jacob et al., 2002).

Deleted: 11

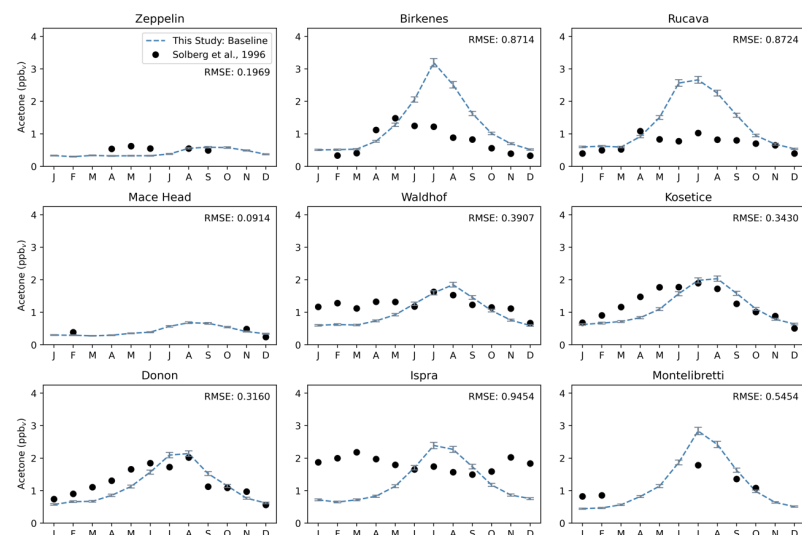


Figure 9. Acetone over twelve months at nine European sites, similar to that of Jacob et al. (2002). The modeled estimates of acetone at the surface from the Baseline simulation are shown as dashed blue lines and the grey error bars represent the one-sigma range of the modeled concentrations in the climatological mean of 5 years. Field measurements from Solberg et al. (1996) are shown as solid black dots. Root mean squared error between the Baseline simulation and field measurements are shown at the top right of each subplot.

Deleted: 11  
Deleted: 1  
Deleted: 1  
Deleted: ,  
Deleted: (left to right, top to bottom): 0.1968, 0.8714, 0.8724, 0.0914, 0.3907, 0.3430, 0.3160, 0.9454, 0.5454.

The GISS ModelE2.1 matches the seasonality of the measurements especially well in Zeppelin, Mace Head, Waldhof, Kosetice, and Donon; the average root mean square error between the Baseline model and the measurements at these five sites are 0.27. The Baseline model overestimates the measurements in Birkenes and Rucava (RMSE  $\approx$  0.87 for both), even though these two sites have low anthropogenic sources. This overestimation has been attributed to the vegetation source, which has a distinct seasonality

Deleted:  $\approx$

i38 and is much stronger than any other source there. Interestingly, in Montelibretti, the model's overestimation of vegetation, yet  
i39 underestimation of local emissions, results in a decent estimation of the sources there (RMSE = 0.53) (Figure 9).

i40  
i41 As mentioned previously, an analysis of the distribution of the regional sources and sinks at the nine European sites shows that,  
i42 except for Zeppelin and Mace Head, all studied European sites have vegetation as the dominant source that strongly contributes to  
i43 the simulated seasonality of concentrations (Figure S7). Vegetation sources peak in the summer months and are lower in the winter.  
i44 Deposition is a major sink of acetone that is comparable in magnitude with the vegetation source. Ocean uptake of acetone follows  
i45 a weak seasonal cycle, being stronger in the summer months. Relatively, the other fluxes (anthropogenic emissions, biomass  
i46 burning and ocean production) do not exhibit much seasonality at these locations (Figure S7).

i47  
i48 We also compared the GISS ModelE2.1's surface acetone at observation sites with less temporal coverage (Figure S8). In general,  
i49 the GISS ModelE2.1 matches the field measurements well. This is especially true for the non-summer seasons in Rosemount and  
i50 Berkeley, USA, and the summer peaks in Utrecht, Netherlands and Mainz, Germany. The model seems to be overestimating  
i51 acetone around Australia, as shown by comparisons with Cape Grim and Wollongong, while underestimating emissions in large  
i52 cities like Shenzhen and Beijing, China, London, UK, and Paris, France (Figure S8).

### i53 3.5 Sensitivity studies

i54 The sensitivity simulations presented here have been described in Section 2.5 and in Table 1. We grouped them in two categories:  
i55 those directly related with chemical sources and sinks, and those related with terrestrial and oceanic acetone fluxes. Overall, the  
i56 sensitivity studies that presented the largest changes to total atmospheric burden included Chem\_Terp0, Chem\_Par0.5,  
i57 Chem\_Par2.0, Veg\_0.7, Ocn\_2.0, and Dep\_fi0 (all but Chem\_Cl0 and BB\_2.0) (Figures S9-S14).

#### i58 3.5.1 Chemistry

i59 Chemistry sensitivity tests that modified the production of acetone were analyzed with respect to the budget and global distribution  
i60 of acetone. In the Chem\_Cl0 simulation, where no acetone oxidation by the chlorine radical occurs, the overall global acetone  
i61 budget does not change. However, in some places like Rucava, Ispra, Montelibretti, and Shenzhen, the shape of the acetone  
i62 concentration profile over the year changes slightly (Figure 10, Figure S15).

Deleted: 454

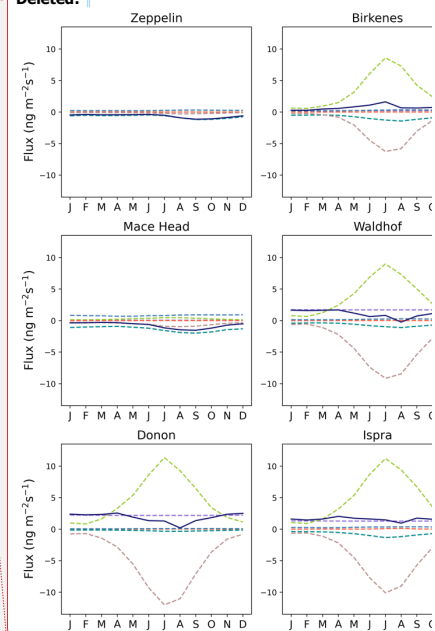
Deleted: 11

Deleted: 12

Deleted: The

Deleted: 12

Deleted: ¶



Deleted: Figure 12. Contribution of acetone sources and sinks in the Baseline simulation over twelve months on the regional level (10° x 12.5° grid boxes) at nine European sites. The sources and sinks are shown as various colored dashed lines, and their sums are shown as a solid navy-blue line. ¶

Deleted: 13

Deleted: ,

Deleted: ¶

... [1]

Deleted: Figure 13. Acetone over twelve months for various sites that do not have enough measurements to resolve seasonality (Australia, Antarctica, Africa, Asia, Europe, North America). ... [2]

Deleted: s

Deleted: 7

Deleted: S12

Deleted: sources

Deleted: 14

Deleted: S13

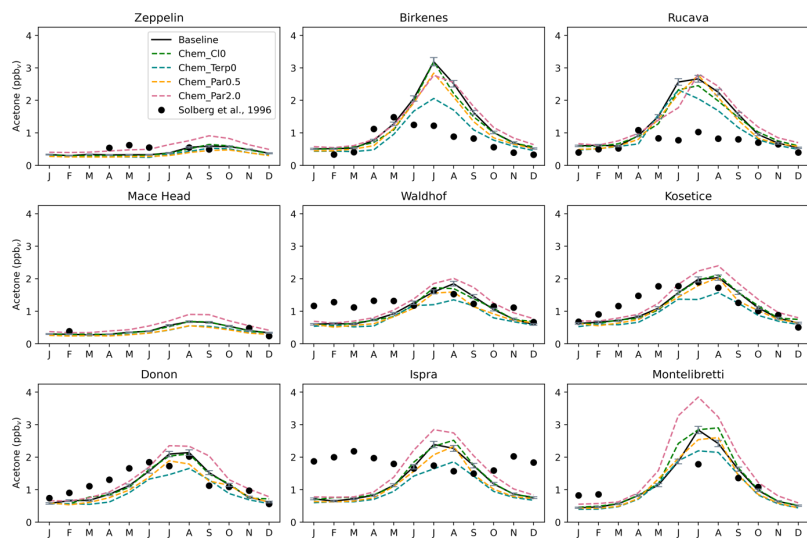


Figure 10. Similar to Figure 9, but with the chemistry sensitivity studies added. The modeled estimates of acetone at the surface from the Baseline simulation are shown as solid black lines, and the sensitivity studies are as follows: removing the acetone + chlorine reaction (dashed green lines), removing the production of acetone from terpenes (dashed blue lines), halving the yield of acetone from paraffin (dashed orange lines), and doubling the yield of acetone from paraffin (dashed pink lines). Field measurements from Solberg et al., (1996) are shown as solid black dots.

The Chem\_Terp0 simulation that removes the production of acetone from terpenes decreases the summer peak of acetone by as much as 35.5% in Birkenes, 25.5% in Mainz, and 25.3% in Berkeley (Figure 10, Figure S15). Other sites like Montelibretti, Ispra and Paris have their summer peak decreased by 22.6%, 22.2%, and 19.0%, respectively (Figure 10, Figure S15). Coastal and remote areas like Zeppelin, Mace Head and Dumont d'Urville, Antarctica are not impacted by the removal of terpenes (Figure 10, Figure S15).

There seems to be some nonlinearities with the relationship between acetone abundance and its yield from paraffin, as the results from the Chem\_Par2.0 and Chem\_Par0.5 simulation reveal that doubling the yield has a stronger impact than halving it. For instance, in Montelibretti, doubling the yield from paraffin increases the summer peak by 35.7%, while halving the yield decreases the summer peak by only 8.3% (Figure 10). A similar relationship is observed at other sites: Ispra (19.1% increase with double paraffin, 2.5% decrease with half paraffin) and Berkeley (12.7% increase with double paraffin, 2.5% decrease with half paraffin) (Figure 10, Figure S15). Overall, we explored chemistry sensitivities that would tend to push acetone in both directions. The Baseline simulation falls between our tests, which we have identified as important uncertainties.

The spatial distribution differences between the chemistry sensitivity studies and the Baseline simulation show some interesting patterns (Figure S16). Removing the production of acetone from terpenes oxidation in the Chem\_Terp0 simulation decreased acetone over the continents, and especially over tropical and boreal forests which are where terpenes are emitted. This change also

Deleted: 14

Deleted: S13

Deleted: 14

Deleted: S13

Deleted: 14

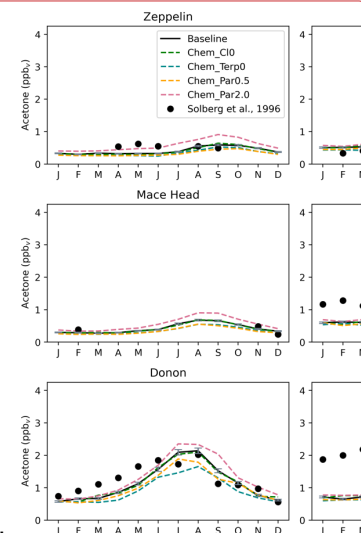
Deleted: S13

Deleted: 14

Deleted: , Figure S13

Deleted: 14

Deleted: S13



Deleted: Figure 14. Similar to Figure 11, but with the chemistry sensitivity studies added. The modelled estimates of acetone at the surface from the Baseline simulation are shown as solid black lines, and the sensitivity studies are as follows: removing the acetone + chlorine reaction (dashed green lines), removing the production of acetone from terpenes (dashed blue lines), halving the yield of acetone from paraffin (dashed orange lines), and doubling the yield of acetone from paraffin (dashed pink lines). Field measurements from Solberg et al., (1996) are shown as solid black dots.

Deleted: (Figure 15)

Formatted: Font: 10 pt, Not Italic, Font color: Text 1



i47 increased acetone concentrations over the oceans due to chemical composition changes downwind that result from the change of  
i48 terpenes oxidation products (Figure S16, top left). Halving production of acetone from paraffin oxidation in the Chem\_Par0.5  
i49 simulation only decreased acetone concentrations over the continents, while doubling it in the Chem\_Par2.0 simulation increased  
i50 acetone concentrations over the continents and strengthened acetone destruction over the tropical oceans (Figure S16, top right and  
i51 bottom middle, respectively). Setting the acetone + chlorine reaction rate to 0 in the Chem\_Cl0 simulation resulted in negligible  
i52 changes across the globe (anomalies of  $<0.4 \text{ ng m}^{-2} \text{ s}^{-1}$ ).

### i53 3.5.2 Terrestrial and oceanic fluxes

i54 Terrestrial and oceanic fluxes sensitivities were analyzed at the same sites. The vegetation flux sensitivity, Veg\_0.7, reduced  
i55 acetone production from MEGAN by 30%. This change decreased the summer peak of acetone down at nearly every location  
i56 studied, but most notably by 32.6% in Birkenes, 22.9% in Rucava, and 22.2% in Rosemount (Figures S17, S18).

i57 ↓  
i58 In the oceanic flux sensitivity simulation, Ocn\_2.0, the concentration of acetone in the water was doubled from 15 nM to 30 nM.  
i59 The results of this simulation varied with geographic location. For instance, in Birkenes, doubling ocean concentration reduced  
i60 overall acetone by 13.9%, while in Montelibretti, it was increased by 16.1% (Figure S17). Even though Birkenes is more of a  
i61 coastal city than Montelibretti, this result may simply be a temperature effect; Birkenes is at 58°N, while Montelibretti is at  
i62 42°N, and a warmer ocean may produce more acetone. Overall, in most places, the doubling ocean acetone concentration did not  
i63 change much atmospheric acetone throughout the year (Figures S17, S18).

i64  
i65 Another broader finding from the ocean sensitivity study is that doubling the ocean acetone concentration impacted oceanic  
i66 emissions of acetone more than the oceanic uptake of acetone (Figure S13). Specifically, in this sensitivity study the emissions  
i67 doubled while the uptake only increased by 40%. This difference may be attributed to the fact that a higher ocean concentration  
i68 will generally cause less resistance in the emission direction, but more resistance in the uptake direction. The differences in  
i69 oceanic acetone emissions and uptakes in this sensitivity study also resulted in increased chemical destruction, and an overall  
i70 higher burden of acetone in the atmosphere (Figure S13).

i71  
i72 In the dry deposition sensitivity simulation, the reactivity factor,  $f_0$ , was reduced from 0.1 to 0. As a result, the amount of acetone  
i73 removed by deposition decreased, and the atmospheric acetone concentration increased. The strongest increases were found to be  
i74 in Ispra (38.4%), Kosetice (37.9%), Paris (37.9%), Beijing (37.3%), Donon (36.6%), Mainz (33.4%), Montelibretti (30.5%),  
i75 Rosemount (28.9%), Berkeley (28.7%), and Waldhof (28.7%) (Figures S17, S18).

i76  
i77 The final terrestrial fluxes sensitivity study, BB\_2.0, doubled biomass burning emissions. This sensitivity did not significantly  
i78 change acetone mixing ratios in any of the locations studied, except an increased summer spike (12.7%) in Birkenes (Figure S17).  
i79 Most of the locations studied were far from biomass burning sites to begin with, however, so an analysis of this sensitivity study  
i80 over biomass burning hotspots is needed.

i81  
i82 The acetone concentration anomalies around the world between the terrestrial and oceanic fluxes sensitivity studies and the  
i83 Baseline simulation are presented in Figure J1. Decreasing acetone production from MEGAN vegetation by 30% resulted in a  
i84 decrease of acetone mixing ratios over the tropical and boreal forests, where this source is most prominent (Figure J1, top left).  
i85 Doubling ocean acetone concentrations increased production of acetone from the oceans globally. This increase was stronger in

Formatted: Font color: Text 1

Formatted: Font: 10 pt, Not Italic, Font color: Text 1

Deleted: This change induced a feedback where acetone concentration increased slightly over the oceans (Figure 15, top left).

Deleted: (Figure 15, top right),

Deleted: but reduced it marginally downwind (Figure 15, bottom). Feedback resulting from this change was that

Deleted: increased

Deleted: tropics

Deleted: ¶ ... [3]

Deleted: Figure 15. Chemistry sensitivities anomalies from ... [4]

Deleted: Figure 16,

Deleted: S14

Deleted: ¶ ... [5]

Deleted: Figure 16. Similar to Figure 11, but with the terre ... [6]

Deleted: 16

Deleted: S11

Deleted: increase

Deleted: increase

Deleted: increase

Deleted: increase

Deleted: increase

Deleted: increase

Deleted: increase

Deleted: increase

Deleted: increase

Deleted: increase

Deleted: increase

Deleted: 16, Figure

Deleted: S14

Deleted: increase

Deleted: 16

Deleted: 17

Deleted: 17

the tropics, due to the higher sea surface temperatures (Figure J1, top right). Reducing the reactivity factor for dry deposition decreased the amount of acetone removed by deposition over the continents (Figure J1, bottom left), in particular where acetone concentration is elevated (Figure 3). Finally, doubling biomass burning emissions did not change acetone mixing ratios much, other than over biomass burning hotspots like central South America, central Africa, Southeast Asia, and Siberia (Figure J1, bottom right).

Deleted: 17  
 Deleted: 17  
 Deleted: 17

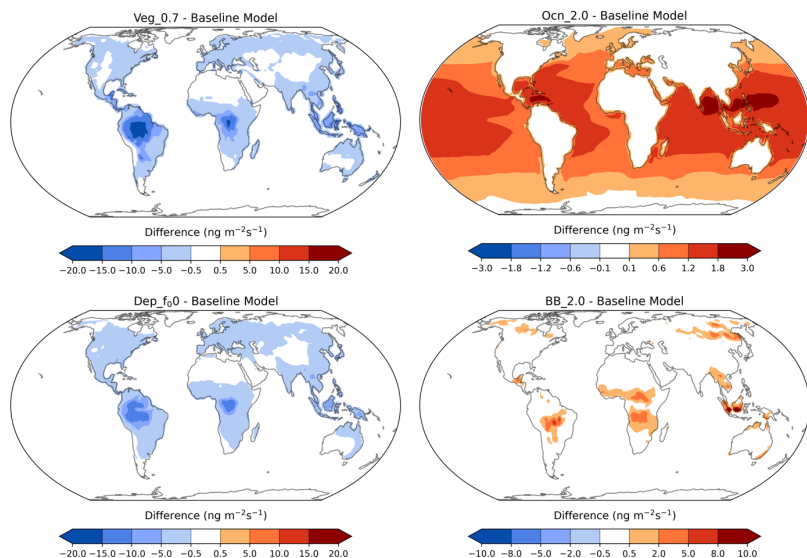


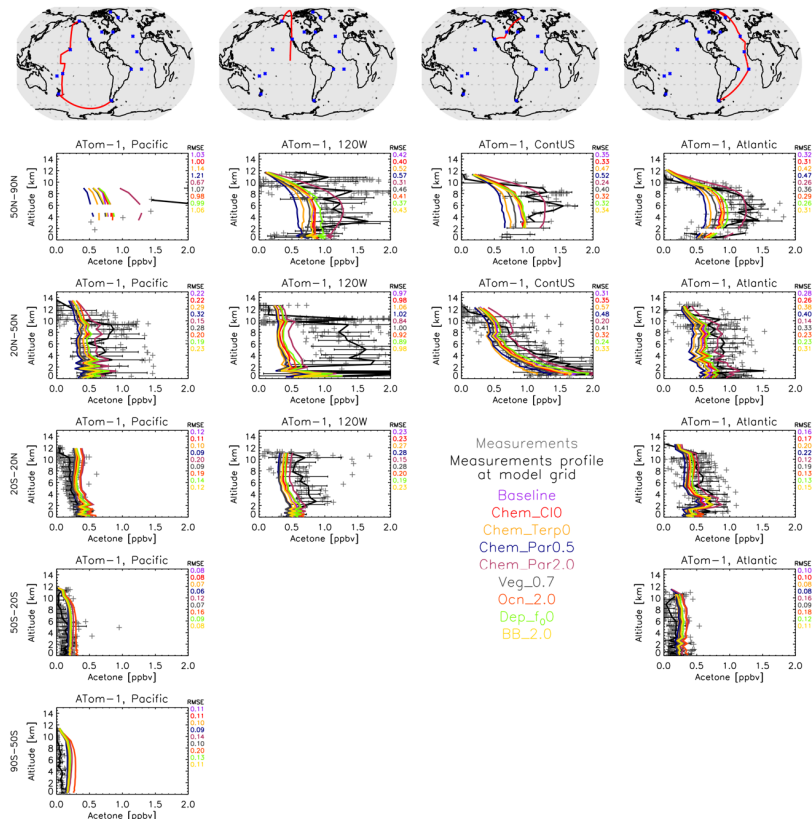
**Figure J1.** Acetone anomalies from the Baseline simulation for the vegetation (top left), ocean (top right), dry deposition (bottom left) and biomass burning (bottom right) sensitivities, with red indicating an increase and blue indicating a decrease of the specific flux. Nonlinear colorbars are used to better differentiate the details in the map.

Deleted: 17

### 3.5.3 ATom comparisons

The ATom comparisons were replicated with the sensitivity simulations (Figure J2, Figures S19-S21). Doubling the paraffin yield of acetone seemed to have the most noticeable impacts on the vertical profiles. As seen during ATom-1 (July-August 2016), doubling the paraffin yield decreases the root mean square error (RMSE) against measurements in the Northern hemisphere polar atmosphere, and brings the model to closer agreement to observations, but decreases the agreement throughout the remote Pacific Ocean, which implies different chemical formation pathways over the more polluted northern hemisphere on the Atlantic Ocean side, compared to the Pacific Ocean. Nearly the exact opposite is calculated in the case of the halving of the paraffin yield of acetone, which adds confidence to the chemical pathway explanation (Figure 12). The doubling of the ocean acetone concentration shows a small improvement (decrease) in the RMSE over the tropical and north Atlantic Ocean during ATom-1 and an even smaller decrease over the north hemisphere Pacific Ocean, but an increase over the tropical and south Pacific Ocean, showing the potential role of different ocean concentrations of acetone across the globe (Figure 12). It needs to be noted though that the model performs fairly well in those regions already, so the small improvements mentioned do not largely affect the regional acetone concentrations, as also expected due to the rather weak acetone source from the ocean.

Deleted: 18  
 Deleted: S15  
 Deleted: S17  
 Deleted: (Figure 18)



167

168 **Figure 12.** Similar to Figure 8, except a comparison between the GISS ModelE2.1 sensitivity simulations and the ATom-1 aircraft  
 169 measurements (July-August 2016). Individual data points are shown with dark grey symbols, and their average values are shown  
 170 in black, with error bars representing the one-sigma range of the averages. The root mean square error (RMSE) of each simulation  
 171 is notes at the top right of each subplot. Note that all sensitivities are to be compared against the Baseline simulation, not the  
 172 Nudged\_ATom one, but as shown earlier this makes very little difference in the comparison with observations (Figure 8).

173

174 The simulations of the boreal winter (January-February 2017) score the best against ATom-2 (Figure S19). Acetone  
 175 concentrations are the lowest during that period in both hemispheres, a direct result from the very low biomass burning  
 176 emissions, which is among the highest acetone sources worldwide. In the region north of 50N, the increase of both the paraffin  
 177 source and the oceanic source of acetone degrade the simulations, and the same applies for the observations around 102W  
 178 longitude, especially at mid-latitudes. The increase in oceanic source over the northern hemisphere mid-latitude Pacific Ocean  
 179 improves (decreases) RMSE, but as already mentioned, the low concentrations of acetone in that area (and in general during  
 180 ATom-2) show that there is small sensitivity in the modified acetone sources to acetone profiles. While the ocean flux may be

Deleted: 18

Deleted: 10

Deleted: dots

Deleted: shown

Deleted: 10

Deleted: (Figure 2)

Deleted: measurements

small, these ATom comparisons reveal that they especially matter in the southern latitudes. These are the same latitudes where the ocean appears to be in equilibrium (neither a strong source nor sink) (Figure 5).

Deleted: 7

During boreal fall (ATom-3), doubling the paraffin yield tends to overshoot most of the observations (Figure S20), contrary to what was calculated during boreal summer (ATom-1; Figure 12). This is the case for most ATom-3 Atlantic Ocean flights, while an improvement is calculated when comparing with the flights near the west coast of the US or the Pacific Ocean mid-latitudes. These results reveal that the model may be underestimating a paraffin source during boreal summer, which diminishes during boreal fall.

Deleted: measurements

Deleted: S1

Deleted: 6

Deleted: 18

The boreal spring season (April-May 2018; ATom-4; Figure S21) is the hardest for the model to simulate when it comes to northern hemisphere concentrations. All sensitivity studies greatly underestimate observations, in particular the long-range transport upper tropospheric amount near the polar latitudes but also the concentrations measured throughout the troposphere at northern mid-latitudes. The model skillfully simulates tropical and southern hemisphere profiles, while it cannot reproduce the higher concentrations at northern latitudes. The increased yield from paraffin or the increased oceanic concentration do reduce RMSE, but still fall short on capturing the magnitude, or the shape, of the profiles of the spring hemisphere. We cannot infer from our model simulations whether this is a missing source or an overestimated sink, but the latter appears to be more plausible, given the large underestimation of all modeled profiles at northern mid-latitudes. In the southern hemisphere, the increase of oceanic acetone clearly degrades model skill, as was frequently the case during the other campaigns presented above. It is worth mentioning that for most cases the changes in the source of acetone do not alter the shape of the vertical profile. This means that the transport or chemical sinks of acetone dictate its spatiotemporal distribution more than sources, while the sources do affect the magnitude of that distribution, quite significantly under some of the sensitivity simulations described here.

Deleted: 17

Deleted: measurements

Deleted: underestimated

Deleted: conditions

#### 4 Conclusion

The development of acetone's representation in the NASA GISS ModelE2.1 from its previous simplistic parameterization of instantaneous isoprene to a full tracer experiencing transport, chemistry, emissions, and deposition of its own, marks a significant improvement to the model's chemical scheme. Calculations of the 3-dimensional distribution of acetone as a function of time, as well as evaluations of its atmospheric burden and source/sink fluxes demonstrate the complexity of acetone's spatiotemporal distribution in the atmosphere. An analysis was conducted to assess the simulated global acetone budget in the context of past modeling studies. Further comparisons were made against field observations on a variety of spatial and temporal scales, which indicated that the model agrees well with surface field measurements and vertical profiles in the remote atmosphere. The chemical formation of acetone from precursor compounds such as paraffin was found to be an uncertain yet impactful factor. Vegetation fluxes as calculated by MEGAN were identified as the dominant acetone source which dictates its seasonality. Additionally, the acetone concentration in seawater was found to affect oceanic sources more than oceanic sinks.

Deleted: extensive

Deleted: measurements

Any feedback between acetone and the rest of the chemistry, and particularly ozone, have not been assessed here, and should be the goal of a future study. Additionally, the current ocean-acetone interaction uses a constant concentration of acetone in the ocean. It will be helpful to test a more realistic, non-uniform ocean acetone concentration, when this becomes available. Finally, other atmospheric conditions such as surface wind speed may be considered further when modifying the ocean scheme.

Deleted: The work presented here demonstrates the usefulness of the approach to evaluate a chemical species in the model and can be used for similar evaluations of other important gaseous and aerosol species.

140 **Code Availability**

141 The GISS ModelE code is publicly available at <https://simplex.giss.nasa.gov/snapshots/>. The most recent public version is E.2.1.2;  
142 the version of the code used here is already committed in the non-public-facing repository and will be released in the future  
143 following the regular release cycle of ModelE, under version E3.1.

144 **Data Availability**

145 We have made available the simulated three-dimensional distributions of acetone from each simulation described in the paper  
146 (Baseline, sensitivity simulations in Table 1, and Nudged\_ATom). These are found in zip files, grouped by simulation, here:  
147 <https://doi.org/10.5281/zenodo.7567614>. Each zip file contains a series of netCDF format files with filenames  
148 {month}\_5yrAvg\_Acetone\_{simulation}.nc, where each file is a climatological average over 5 years of repeated forcing  
149 conditions.

150  
151 The exception is the transient-forcing simulation "Nudged\_ATom", which contains single-month averages of acetone from JUL  
152 2016 through MAY 2018, to cover the ATom observational period. The file names for that simulation are of the form:  
153 {month}\_{year}\_Acetone\_Nudged\_ATom.nc. Acetone is in ppb, units and given on the model's native grid and vertical levels.  
154 These are hybrid sigma levels, but nominal pressure middles and edges are given in the plm and ple variables, respectively, and  
155 the grid box surface areas are also provided.

156 **Author Contribution**

157 KT conceived the study and guided the model development which was done by GF. All simulations presented here were performed  
158 by GF. DS advised during the whole development process. AR did the literature search and all comparisons against other modeling  
159 studies. With the exception of the ATom analysis and plots which were done by KT, and comparisons against field measurements  
160 and the rest of the plots were done by AR. AR drafted the first version of the manuscript, and all authors contributed to it. GF  
161 prepared all model outputs for dissemination.

162 **Competing Interests**

163 The authors declare that they have no conflict of interest.

164 **Acknowledgements**

165 Climate modeling at GISS is supported by the NASA Modeling, Analysis and Prediction program. AR acknowledges support from  
166 North Carolina Space Grant and the NASA Office of STEM Engagement. Resources supporting this work were provided by the  
167 NASA High-End Computing (HEC) Program through the NASA Center for Climate Simulation (NCCS) at Goddard Space Flight  
168 Center.

169 **References**

170 Apel, E. C., Asher, E. C., Hills, A. J., and Hornbrook, R. S.: ATom: Volatile Organic Compounds (VOCs) from the TOGA  
171 instrument, Version 2, ORNL DAAC, <https://doi.org/10.3334/ORNLDAAC/1936>, 2021.

**Deleted:** ¶  
The 3-dimensional model output of acetone concentrations will be made public at the GISS website at the time of publication in the discussion phase, as was done in other publications (e.g. <https://pubs.giss.nasa.gov/abs/ba08500g.html>). This statement will be modified accordingly for final publication. ¶

**Formatted:** Heading 1

**Deleted:**

**Deleted:** <https://doi.org/10.5281/zenodo.7567614>

880 Arnold, S. R., Chipperfield, M. P., and Blitz, M. A.: A three-dimensional model study of the effect of new temperature-dependent  
881 quantum yields for acetone photolysis, *J. Geophys. Res. Atmospheres*, 110, <https://doi.org/10.1029/2005JD005998>, 2005.

882 Beale, R., Dixon, J. L., Arnold, S. R., Liss, P. S., and Nightingale, P. D.: Methanol, acetaldehyde, and acetone in the surface waters  
883 of the Atlantic Ocean, *J. Geophys. Res. Oceans*, 118, 5412–5425, <https://doi.org/10.1002/jgrc.20322>, 2013.

884 Benkelberg, H.-J., Hamm, S., and Warnecke, P.: Henry's law coefficients for aqueous solutions of acetone, acetaldehyde and  
885 acetonitrile, and equilibrium constants for the addition compounds of acetone and acetaldehyde with bisulfite, *J. Atmospheric*  
886 *Chem.*, 20, 17–34, <https://doi.org/10.1007/BF01099916>, 1995.

887 Brewer, J. F., Bishop, M., Kelp, M., Keller, C. A., Ravishankara, A. R., and Fischer, E. V.: A sensitivity analysis of key natural  
888 factors in the modeled global acetone budget, *J. Geophys. Res. Atmospheres*, 122, 2043–2058,  
889 <https://doi.org/10.1002/2016JD025935>, 2017.

890 Chin, M., Jacob, D. J., Gardner, G. M., Foreman-Fowler, M. S., Spiro, P. A., and Savoie, D. L.: A global three-dimensional model  
891 of tropospheric sulfate, *J. Geophys. Res. Atmospheres*, 101, 18667–18690, <https://doi.org/10.1029/96JD01221>, 1996.

892 Dolgorouky, C., Gros, V., Sarda-Esteve, R., Sinha, V., Williams, J., Marchand, N., Sauvage, S., Poulain, L., Sciare, J., and  
893 Bonsang, B.: Total OH reactivity measurements in Paris during the 2010 MEGAPOLI winter campaign, *Atmospheric Chem. Phys.*,  
894 12, 9593–9612, <https://doi.org/10.5194/acp-12-9593-2012>, 2012.

895 Dufour, G., Szopa, S., Harrison, J. J., Boone, C. D., and Bernath, P. F.: Seasonal variations of acetone in the upper troposphere–  
896 lower stratosphere of the northern midlatitudes as observed by ACE-FTS, *J. Mol. Spectrosc.*, 323, 67–77,  
897 <https://doi.org/10.1016/j.jms.2016.02.006>, 2016.

898 Elias, T., Szopa, S., Zahn, A., Schuck, T., Brenninkmeijer, C., Sprung, D., and Slemr, F.: Acetone variability in the upper  
899 troposphere: analysis of CARIBIC observations and LMDz-INCA chemistry-climate model simulations, *Atmospheric Chem.*  
900 *Phys.*, 11, 8053–8074, <https://doi.org/10.5194/acp-11-8053-2011>, 2011.

901 Fischbeck, G., Bönisch, H., Neumaier, M., Brenninkmeijer, C. A. M., Orphal, J., Brito, J., Becker, J., Sprung, D., van Velthoven,  
902 P. F. J., and Zahn, A.: Acetone–CO enhancement ratios in the upper troposphere based on 7 years of CARIBIC data: new insights  
903 and estimates of regional acetone fluxes, *Atmospheric Chem. Phys.*, 17, 1985–2008, <https://doi.org/10.5194/acp-17-1985-2017>,  
904 2017.

905 Fischer, E. V., Jacob, D. J., Millet, D. B., Yantosca, R. M., and Mao, J.: The role of the ocean in the global atmospheric budget of  
906 acetone, *Geophys. Res. Lett.*, 39, <https://doi.org/10.1029/2011GL050086>, 2012.

907 Folberth, G. A., Hauglustaine, D. A., Lathière, J., and Brocheton, F.: Interactive chemistry in the Laboratoire de Météorologie  
908 Dynamique general circulation model: model description and impact analysis of biogenic hydrocarbons on tropospheric chemistry,  
909 *Atmospheric Chem. Phys.*, 6, 2273–2319, <https://doi.org/10.5194/acp-6-2273-2006>, 2006.

910 Fujimori, S., Hasegawa, T., Masui, T., Takahashi, K., Herran, D. S., Dai, H., Hijioka, Y., and Kainuma, M.: SSP3: AIM  
911 implementation of Shared Socioeconomic Pathways, *Glob. Environ. Change*, 42, 268–283,  
912 <https://doi.org/10.1016/j.gloenvcha.2016.06.009>, 2017.

913 Galbally, I., Lawson, S. J., Bentley, S., Gillett, R., Meyer, M., and Goldstein, A.: Volatile organic compounds in marine air at Cape  
914 Grim, Australia, *Environ. Chem. - Env. CHEM*, 4, <https://doi.org/10.1071/EN07024>, 2007.

915 Gelaro, R., McCarty, W., Suárez, M. J., Todling, R., Molod, A., Takacs, L., Randles, C. A., Darmenov, A., Bosilovich, M. G.,  
916 Reichle, R., Wargan, K., Coy, L., Cullather, R., Draper, C., Akella, S., Buchard, V., Conaty, A., Silva, A. M. da, Gu, W., Kim, G.-  
917 K., Koster, R., Lucchesi, R., Merkova, D., Nielsen, J. E., Partyka, G., Pawson, S., Putman, W., Rienecker, M., Schubert, S. D.,  
918 Sienkiewicz, M., and Zhao, B.: The Modern-Era Retrospective Analysis for Research and Applications, Version 2 (MERRA-2),  
919 *J. Clim.*, 30, 5419–5454, <https://doi.org/10.1175/JCLI-D-16-0758.1>, 2017.

920 de Gouw, J., Warneke, C., Holzinger, R., Klüpfel, T., and Williams, J.: Inter-comparison between airborne measurements of  
921 methanol, acetonitrile and acetone using two differently configured PTR-MS instruments, *Int. J. Mass Spectrom.*, 239, 129–137,  
922 <https://doi.org/10.1016/j.jms.2004.07.025>, 2004.

123 Guenther, A. B., Jiang, X., Heald, C. L., Sakulyanontvittaya, T., Duhl, T., Emmons, L. K., and Wang, X.: The Model of Emissions  
124 of Gases and Aerosols from Nature version 2.1 (MEGAN2.1): an extended and updated framework for modeling biogenic  
125 emissions, *Geosci. Model Dev.*, 5, 1471–1492, <https://doi.org/10.5194/gmd-5-1471-2012>, 2012.

126 Guérette, É.-A., Paton-Walsh, C., Galbally, I., Molloy, S., Lawson, S., Kubistin, D., Buchholz, R., Griffith, D. W. T., Langenfelds,  
127 R. L., Krummel, P. B., Loh, Z., Chambers, S., Griffiths, A., Keywood, M., Selleck, P., Dominick, D., Humphries, R., and Wilson,  
128 S. R.: Composition of Clean Marine Air and Biogenic Influences on VOCs during the MUMBA Campaign, *Atmosphere*, 10, 383,  
129 <https://doi.org/10.3390/atmos10070383>, 2019.

130 Hoelsy, R. M., Smith, S. J., Feng, L., Klimont, Z., Janssens-Maenhout, G., Pitkanen, T., Seibert, J. J., Vu, L., Andres, R. J., Bolt,  
131 R. M., Bond, T. C., Dawidowski, L., Kholod, N., Kurokawa, J., Li, M., Liu, L., Lu, Z., Moura, M. C. P., O'Rourke, P. R., and  
132 Zhang, Q.: Historical (1750–2014) anthropogenic emissions of reactive gases and aerosols from the Community Emissions Data  
133 System (CEDS), *Geosci. Model Dev.*, 11, 369–408, <https://doi.org/10.5194/gmd-11-369-2018>, 2018.

134 Hu, L., Millet, D. B., Kim, S. Y., Wells, K. C., Griffis, T. J., Fischer, E. V., Helmig, D., Hueber, J., and Curtis, A. J.: North  
135 American acetone sources determined from tall tower measurements and inverse modeling, *Atmospheric Chem. Phys.*, 13, 3379–  
136 3392, <https://doi.org/10.5194/acp-13-3379-2013>, 2013.

137 Huang, X.-F., Zhang, B., Xia, S.-Y., Han, Y., Wang, C., Yu, G.-H., and Feng, N.: Sources of oxygenated volatile organic  
138 compounds (OVOCs) in urban atmospheres in North and South China, *Environ. Pollut.*, 261, 114152,  
139 <https://doi.org/10.1016/j.envpol.2020.114152>, 2020.

140 Jacob, D. J., Field, B. D., Jin, E. M., Bey, I., Li, Q., Logan, J. A., Yantosca, R. M., and Singh, H. B.: Atmospheric budget of  
141 acetone, *J. Geophys. Res. Atmospheres*, 107, ACH 5-1-ACH 5-17, <https://doi.org/10.1029/2001JD000694>, 2002.

142 Johnson, M. T.: A numerical scheme to calculate temperature and salinity dependent air-water transfer velocities for any gas,  
143 *Ocean Sci.*, 6, 913–932, <https://doi.org/10.5194/os-6-913-2010>, 2010.

144 Kelley, M., Schmidt, G. A., Nazarenko, L. S., Bauer, S. E., Ruedy, R., Russell, G. L., Ackerman, A. S., Aleinov, I., Bauer, M.,  
145 Bleck, R., Canuto, V., Cesana, G., Cheng, Y., Clune, T. L., Cook, B. I., Cruz, C. A., Genio, A. D. D., Elsaesser, G. S., Faluvegi,  
146 G., Kiang, N. Y., Kim, D., Lacis, A. A., Leboissetier, A., LeGrande, A. N., Lo, K. K., Marshall, J., Matthews, E. E., McDermid,  
147 S., Mezunman, K., Miller, R. L., Murray, L. T., Oinas, V., Orbe, C., Garcia-Pando, C. P., Perlwitz, J. P., Puma, M. J., Rind, D.,  
148 Romanou, A., Shindell, D. T., Sun, S., Tausnev, N., Tsigaridis, K., Tselioudis, G., Weng, E., Wu, J., and Yao, M.-S.: GISS-E2.1:  
149 Configurations and Climatology, *J. Adv. Model. Earth Syst.*, 12, e2019MS002025, <https://doi.org/10.1029/2019MS002025>, 2020.

150 Khan, M. A. H., Cooke, M. C., Utembe, S. R., Archibald, A. T., Maxwell, P., Morris, W. C., Xiao, P., Derwent, R. G., Jenkin, M.  
151 E., Percival, C. J., Walsh, R. C., Young, T. D. S., Simmonds, P. G., Nickless, G., O'Doherty, S., and Shallcross, D. E.: A study of  
152 global atmospheric budget and distribution of acetone using global atmospheric model STOCHEM-CRI, *Atmos. Environ.*, 112,  
153 269–277, <https://doi.org/10.1016/j.atmosenv.2015.04.056>, 2015.

154 Koch, D., Jacob, D., Tegen, I., Rind, D., and Chin, M.: Tropospheric sulfur simulation and sulfate direct radiative forcing in the  
155 Goddard Institute for Space Studies general circulation model, *J. Geophys. Res. Atmospheres*, 104, 23799–23822,  
156 <https://doi.org/10.1029/1999JD900248>, 1999.

157 Langford, B., Nemitz, E., House, E., Phillips, G. J., Famulari, D., Davison, B., Hopkins, J. R., Lewis, A. C., and Hewitt, C. N.:  
158 Fluxes and concentrations of volatile organic compounds above central London, UK, *Atmospheric Chem. Phys.*, 10, 627–645,  
159 <https://doi.org/10.5194/acp-10-627-2010>, 2010.

160 Lewis, A. C., Hopkins, J. R., Carpenter, L. J., Stanton, J., Read, K. A., and Pilling, M. J.: Sources and sinks of acetone, methanol,  
161 and acetaldehyde in North Atlantic marine air, *Atmospheric Chem. Phys.*, 5, 1963–1974, <https://doi.org/10.5194/acp-5-1963-2005>,  
162 2005.

163 Li, K., Li, J., Tong, S., Wang, W., Huang, R.-J., and Ge, M.: Characteristics of wintertime VOCs in suburban and urban Beijing:  
164 concentrations, emission ratios, and festival effects, *Atmospheric Chem. Phys.*, 19, 8021–8036, <https://doi.org/10.5194/acp-19-8021-2019>, 2019.

166 Liss, P. S. and Slater, P. G.: Flux of Gases across the Air-Sea Interface, *Nature*, 247, 181–184, <https://doi.org/10.1038/247181a0>,  
167 1974.

168 Marandino, C. A., Bruyn, W. J. D., Miller, S. D., Prather, M. J., and Saltzman, E. S.: Oceanic uptake and the global atmospheric  
169 acetone budget, *Geophys. Res. Lett.*, 32, <https://doi.org/10.1029/2005GL023285>, 2005.

170 van Marle, M. J. E., Kloster, S., Magi, B. I., Marlon, J. R., Daniiau, A.-L., Field, R. D., Arneth, A., Forrest, M., Hantson, S.,  
171 Kehrwald, N. M., Knorr, W., Lasslop, G., Li, F., Mangeon, S., Yue, C., Kaiser, J. W., and van der Werf, G. R.: Historic global  
172 biomass burning emissions for CMIP6 (BB4CMIP) based on merging satellite observations with proxies and fire models (1750–  
173 2015), *Geosci. Model Dev.*, 10, 3329–3357, <https://doi.org/10.5194/gmd-10-3329-2017>, 2017.

174 Met Office, Hadley Centre: HadISST 1.1 - Global sea-ice coverage and SST (1870-Present), [\[Internet\]. NCAS British  
175 Atmospheric Data Centre 2006, April 3, 2021. Available from  
176 http://badc.nerc.ac.uk/view/badc.nerc.ac.uk\\_ATOM\\_dataent\\_hadisst\\_2006](http://badc.nerc.ac.uk/view/badc.nerc.ac.uk_ATOM_dataent_hadisst_2006).

177 Neu, J. L., Prather, M. J., and Penner, J. E.: Global atmospheric chemistry: Integrating over fractional cloud cover, *J. Geophys.*  
178 *Res. Atmospheres*, 112, 2006JD008007, <https://doi.org/10.1029/2006JD008007>, 2007.

179 O'Rourke, P. R., Smith, S. J., Mott, A., Ahsan, H., McDuffie, E. E., Crippa, M., Klimont, Z., McDonald, B., Wang, S., Nicholson,  
180 M. B., Feng, L., and Hoesly, R. M.: CEDS v\_2021\_04\_21 Release Emission Data, <https://doi.org/10.5281/zenodo.4741285>, 2021.

181 Read, K. A., Carpenter, L. J., Arnold, S. R., Beale, R., Nightingale, P. D., Hopkins, J. R., Lewis, A. C., Lee, J. D., Mendes, L., and  
182 Pickering, S. J.: Multiannual Observations of Acetone, Methanol, and Acetaldehyde in Remote Tropical Atlantic Air: Implications  
183 for Atmospheric OVOC Budgets and Oxidative Capacity, *Environ. Sci. Technol.*, 46, 11028–11039,  
184 <https://doi.org/10.1021/es302082p>, 2012.

185 Riahi, K., van Vuuren, D. P., Kriegler, E., Edmonds, J., O'Neill, B. C., Fujimori, S., Bauer, N., Calvin, K., Dellink, R., Fricko, O.,  
186 Lutz, W., Popp, A., Cuaresma, J. C., Ke, S., Leimbach, M., Jiang, L., Kram, T., Rao, S., Emmerling, J., Ebi, K., Hasegawa, T.,  
187 Havlik, P., Humpenöder, F., Da Silva, L. A., Smith, S., Stehfest, E., Bosetti, V., Eom, J., Gernaat, D., Masui, T., Rogelj, J., Strefler,  
188 J., Drouet, L., Krey, V., Luderer, G., Harmsen, M., Takahashi, K., Baumstark, L., Doelman, J. C., Kainuma, M., Klimont, Z.,  
189 Marangoni, G., Lotze-Campen, H., Obersteiner, M., Tabeau, A., and Tavoni, M.: The Shared Socioeconomic Pathways and their  
190 energy, land use, and greenhouse gas emissions implications: An overview, *Glob. Environ. Change*, 42, 153–168,  
191 <https://doi.org/10.1016/j.gloenvcha.2016.05.009>, 2017.

192 Sander, R.: *Compilation of Henry's Law Constants for Inorganic and Organic Species of Potential Importance in Environmental  
193 Chemistry*, 1999.

194 Sander, S. P., J. Abbatt, J. R. Barker, J. B. Burkholder, R. R. Friedl, D. M. Golden, R. E. Huie, C. E. Kolb, M. J. Kurylo, G. K.  
195 Moortgat, V. L. Orkin, and P. H. Wine: *Chemical Kinetics and Photochemical Data for Use in Atmospheric Studies Evaluation  
196 No. 17*, JPL Publication 10-6, Jet Propulsion Laboratory, Pasadena, 2011.

197 Schade, G. W. and Goldstein, A. H.: Seasonal measurements of acetone and methanol: Abundances and implications for  
198 atmospheric budgets, *Glob. Biogeochem. Cycles*, 20, <https://doi.org/10.1029/2005GB002566>, 2006.

199 Shindell, D. T., Grenfell, J. L., Rind, D., Grewe, V., and Price, C.: Chemistry-climate interactions in the Goddard Institute for  
200 Space Studies general circulation model: 1. Tropospheric chemistry model description and evaluation, *J. Geophys. Res.*  
201 *Atmospheres*, 106, 8047–8075, <https://doi.org/10.1029/2000JD900704>, 2001.

202 Shindell, D. T., Faluvegi, G., and Bell, N.: Preindustrial-to-present-day radiative forcing by tropospheric ozone from improved  
203 simulations with the GISS chemistry-climate GCM, *Atmospheric Chem. Phys.*, 3, 1675–1702, [https://doi.org/10.5194/acp-3-1675-  
204 2003](https://doi.org/10.5194/acp-3-1675-2003), 2003.

205 Singh, H., Chen, Y., Tabazadeh, A., Fukui, Y., Bey, I., Yantosca, R., Jacob, D., Arnold, F., Wohlfrom, K., Atlas, E., Flocke, F.,  
206 Blake, D., Blake, N., Heikes, B., Snow, J., Talbot, R., Gregory, G., Sachse, G., Vay, S., and Kondo, Y.: Distribution and fate of  
207 selected oxygenated organic species in the troposphere and lower stratosphere over the Atlantic, *J. Geophys. Res. Atmospheres*,  
208 105, 3795–3805, <https://doi.org/10.1029/1999JD900779>, 2000.

209 Singh, H. B., O'Hara, D., Herlth, D., Sachse, W., Blake, D. R., Bradshaw, J. D., Kanakidou, M., and Crutzen, P. J.: Acetone in the  
210 atmosphere: Distribution, sources, and sinks, *J. Geophys. Res. Atmospheres*, 99, 1805–1819, <https://doi.org/10.1029/93JD00764>,  
211 1994.



112 Singh, H. B., Tabazadeh, A., Evans, M. J., Field, B. D., Jacob, D. J., Sachse, G., Crawford, J. H., Shetter, R., and Brune, W. H.:  
113 Oxygenated volatile organic chemicals in the oceans: Inferences and implications based on atmospheric observations and air-sea  
114 exchange models, *Geophys. Res. Lett.*, 30, <https://doi.org/10.1029/2003GL017933>, 2003.

115 Singh, H. B., Salas, L. J., Chatfield, R. B., Czech, E., Fried, A., Walega, J., Evans, M. J., Field, B. D., Jacob, D. J., Blake, D.,  
116 Heikes, B., Talbot, R., Sachse, G., Crawford, J. H., Avery, M. A., Sandholm, S., and Fuelberg, H.: Analysis of the atmospheric  
117 distribution, sources, and sinks of oxygenated volatile organic chemicals based on measurements over the Pacific during TRACE-  
118 P, *J. Geophys. Res. Atmospheres*, 109, <https://doi.org/10.1029/2003JD003883>, 2004.

119 Solberg, S., Dye, C., Schmidbauer, N., Herzog, A., and Gehrige, R.: Carbonyls and nonmethane hydrocarbons at rural European  
120 sites from the mediterranean to the arctic, *J. Atmospheric Chem.*, 25, 33–66, <https://doi.org/10.1007/BF00053285>, 1996.

121 Taylor, K., Williamson, D., and Zwiers, F.: The sea surface temperature and sea ice concentration boundary conditions for AMIP  
122 II simulations, [PCMDI Report 60](#), Program for Climate Model Diagnosis and Intercomparison, Lawrence Livermore National  
123 Laboratory, 2000.

124 Thompson, C. R., Wofsy, S. C., Prather, M. J., Newman, P. A., Hanisco, T. F., Ryerson, T. B., Fahey, D. W., Apel, E. C., Brock,  
125 C. A., Brune, W. H., Froyd, K., Katich, J. M., Nicely, J. M., Peischl, J., Ray, E., Veres, P. R., Wang, S., Allen, H. M., Asher, E.,  
126 Bian, H., Blake, D., Bourgeois, I., Budney, J., Bui, T. P., Butler, A., Campuzano-Jost, P., Chang, C., Chin, M., Commane, R.,  
127 Correa, G., Crouse, J. D., Daube, B., Dibb, J. E., DiGangi, J. P., Diskin, G. S., Dollner, M., Elkins, J. W., Fiore, A. M., Flynn, C.  
128 M., Guo, H., Hall, S. R., Hannun, R. A., Hills, A., Hints, E. J., Hodzic, A., Hornbrook, R. S., Huey, L. G., Jimenez, J. L., Keeling,  
129 R. F., Kim, M. J., Kuep, A., Lacey, F., Lait, L. R., Lamarque, J.-F., Liu, J., McKain, K., Meinardi, S., Miller, D. O., Montzka, S.  
130 A., Moore, F. L., Morgan, E. J., Murphy, D. M., Murray, L. T., Nault, B. A., Neuman, J. A., Nguyen, L., Gonzalez, Y., Rollins,  
131 A., Rosenlof, K., Sargent, M., Schill, G., Schwarz, J. P., Clair, J. M. S., Steenrod, S. D., Stephens, B. B., Strahan, S. E., Strode, R.  
132 A., Sweeney, C., Thames, A. B., Ullmann, K., Wagner, N., Weber, R., Weinzierl, B., Wennberg, P. O., Williamson, C. J., Wolfe,  
133 G. M., and Zeng, L.: The NASA Atmospheric Tomography (ATom) Mission: Imaging the Chemistry of the Global Atmosphere,  
134 *Bull. Am. Meteorol. Soc.*, 103, E761–E790, <https://doi.org/10.1175/BAMS-D-20-0315.1>, 2022.

135 Tsigaridis, K. and Kanakidou, M.: Global modelling of secondary organic aerosol in the troposphere: a sensitivity analysis, *Atmos*  
136 *Chem Phys*, 2003.

137 Wang, S., Apel, E. C., Schwantes, R. H., Bates, K. H., Jacob, D. J., Fischer, E. V., Hornbrook, R. S., Hills, A. J., Emmons, L. K.,  
138 Pan, L. L., Honomichl, S., Tilmes, S., Lamarque, J.-F., Yang, M., Marandino, C. A., Saltzman, E. S., Bruyn, W. de, Kameyama,  
139 S., Tanimoto, H., Omori, Y., Hall, S. R., Ullmann, K., Ryerson, T. B., Thompson, C. R., Peischl, J., Daube, B. C., Commane, R.,  
140 McKain, K., Sweeney, C., Thames, A. B., Miller, D. O., Brune, W. H., Diskin, G. S., DiGangi, J. P., and Wofsy, S. C.: Global  
141 Atmospheric Budget of Acetone: Air-Sea Exchange and the Contribution to Hydroxyl Radicals, *J. Geophys. Res. Atmospheres*,  
142 125, e2020JD032553, <https://doi.org/10.1029/2020JD032553>, 2020.

143 Warneke, C. and de Gouw, J. A.: Organic trace gas composition of the marine boundary layer over the northwest Indian Ocean in  
144 April 2000, *Atmos. Environ.*, 35, 5923–5933, [https://doi.org/10.1016/S1352-2310\(01\)00384-3](https://doi.org/10.1016/S1352-2310(01)00384-3), 2001.

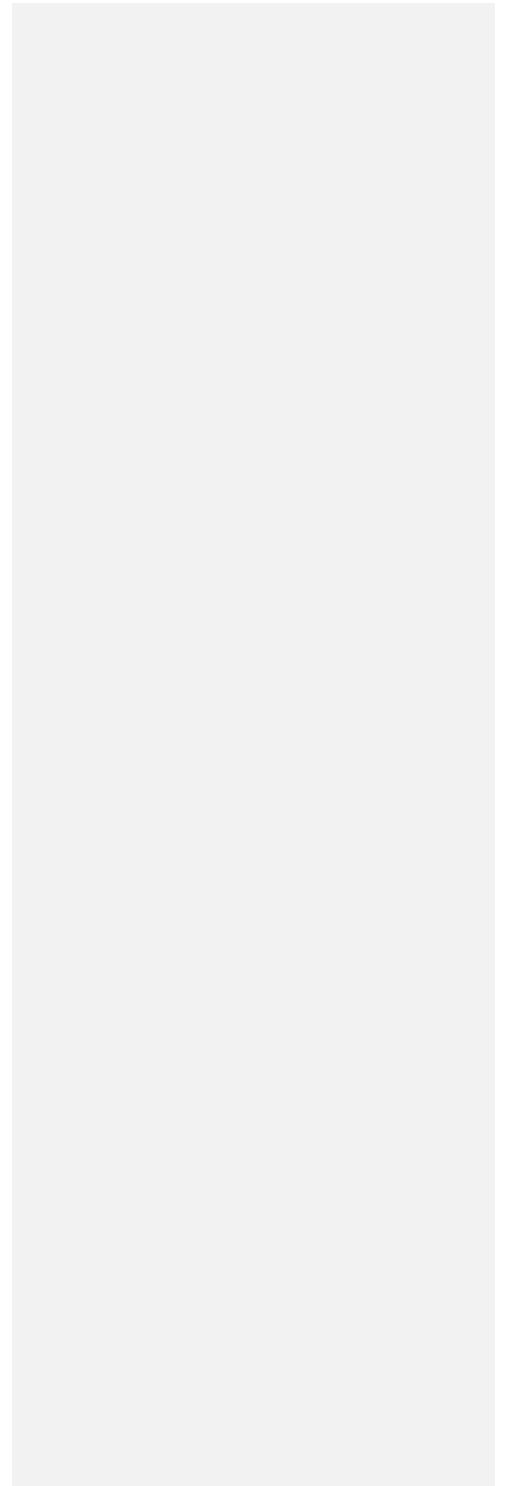
145 Weimer, M., Schröter, J., Eckstein, J., Deetz, K., Neumaier, M., Fischbeck, G., Hu, L., Millet, D. B., Rieger, D., Vogel, H., Vogel,  
146 B., Reddmann, T., Kirner, O., Ruhnke, R., and Braesicke, P.: An emission module for ICON-ART 2.0: implementation and  
147 simulations of acetone, *Geosci. Model Dev.*, 10, 2471–2494, <https://doi.org/10.5194/gmd-10-2471-2017>, 2017.

148 Wesely, M. L. and Hicks, B. B.: Some Factors that Affect the Deposition Rates of Sulfur Dioxide and Similar Gases on Vegetation,  
149 *J. Air Pollut. Control Assoc.*, 27, 1110–1116, <https://doi.org/10.1080/00022470.1977.10470534>, 1977.

150 Yoshino, A., Nakashima, Y., Miyazaki, K., Kato, S., Suthawaree, J., Shimo, N., Matsunaga, S., Chatani, S., Apel, E., Greenberg,  
151 J., Guenther, A., Ueno, H., Sasaki, H., Hoshi, J., Yokota, H., Ishii, K., and Kajii, Y.: Air quality diagnosis from comprehensive  
152 observations of total OH reactivity and reactive trace species in urban central Tokyo, *Atmos. Environ.*, 49, 51–59,  
153 <https://doi.org/10.1016/j.atmosenv.2011.12.029>, 2012.

154 Yuan, B., Hu, W. W., Shao, M., Wang, M., Chen, W. T., Lu, S. H., Zeng, L. M., and Hu, M.: VOC emissions, evolutions and  
155 contributions to SOA formation at a receptor site in eastern China, *Atmospheric Chem. Phys.*, 13, 8815–8832,  
156 <https://doi.org/10.5194/acp-13-8815-2013>, 2013.

157 Zhou, X. and Mopper, K.: Apparent partition coefficients of 15 carbonyl compounds between air and seawater and between air  
158 and freshwater; implications for air-sea exchange, *Environ. Sci. Technol.*, 24, 1864–1869, <https://doi.org/10.1021/es00082a013>,  
159 1990.



▼  
▲  
**Page 15: [1] Deleted**      **Alexandra Rivera**      **2/1/24 3:32:00 PM**  
x

▼  
▲  
**Page 15: [2] Deleted**      **Alexandra Rivera**      **2/1/24 3:29:00 PM**  
x

▼  
▲  
**Page 17: [3] Deleted**      **Alexandra Rivera**      **2/1/24 3:39:00 PM**  
x

▼  
▲  
**Page 17: [4] Deleted**      **Alexandra Rivera**      **2/1/24 3:39:00 PM**  
x

▼  
▲  
**Page 17: [5] Deleted**      **Alexandra Rivera**      **2/1/24 4:23:00 PM**  
x

▼  
▲  
**Page 17: [6] Deleted**      **Alexandra Rivera**      **2/1/24 4:22:00 PM**  
x